JAAS

CRITICAL REVIEW

View Article Online
View Journal | View Issue

Cite this: *J. Anal. At. Spectrom.*, 2020, **35**, 1740

A critical review of single particle inductively coupled plasma mass spectrometry – A step towards an ideal method for nanomaterial characterization†

Darya Mozhayeva [a] and Carsten Engelhard *[ab]

Single particle inductively coupled plasma mass spectrometry (spICP-MS or SP-ICP-MS depending on the author) is becoming an important tool for the characterization of nanoparticles (NPs). The method allows determining the size, size distribution, and particle number concentrations of NPs in suspensions after a mere few minutes of measurement. This review is modeled after the concept of "an ideal method for atomic spectroscopy" introduced by Gary M. Hieftje in his publication dedicated to Howard Malmstadt. This review discusses the instrumental developments in spICP-MS of recent years step-by-step, from the sample introduction system to the detector. The authors identify necessary improvements and suggest directions for further developments which have the potential to bring the method closer to "an ideal method for atomic spectroscopy". The review also discusses the literature on coupling spICP-MS to separation and fractionation techniques including capillary electrophoresis (CE), field flow fractionation (FFF), and differential mobility analysis (DMA). The second part of the review is dedicated to the applications of spICP-MS. Key steps in sample preparation and selected instrumental conditions that were used in the published literature are summarized in a tabular form. Most frequently, spICP-MS is used for silver (Ag), gold (Au), and titanium dioxide (TiO_2) nanomaterial analysis. Data acquisition was typically performed with millisecond dwell times in the past while a time resolution of hundreds of microseconds has been used more often in the last five years. The table may serve as a guide to choose an experimental procedure depending on the matrix that is present in the sample under investigation.

Received 17th June 2019
Accepted 25th July 2019

DOI: 10.1039/c9ja00206e

rsc.li/jaas

[a]*Department of Chemistry and Biology, University of Siegen, Adolf-Reichwein-Str. 2, D-57076 Siegen, Germany. E-mail: engelhard@chemie.uni-siegen.de; Fax: +492717402041*

[b]*Center of Micro- and Nanochemistry and Engineering, University of Siegen, Adolf-Reichwein-Str. 2, D-57076 Siegen, Germany*

† Dedicated to Professor Gary M. Hieftje on the occasion of his retirement from Indiana University.

Darya Mozhayeva received her B.Sc. in Chemistry (2013) from Al-Farabi Kazakh National University, Kazakhstan, and her M.Sc. in Chemistry (2015) from the University of Siegen, Germany. In 2019, she received a Dr rer. nat. degree in Analytical Chemistry from the University of Siegen. Her graduate work was focused on the development and optimization of capillary electrophoresis coupled to spICP-MS for nanomaterial applications and fundamental studies thereof.

Carsten Engelhard is a Professor of Analytical Chemistry in the Department of Chemistry and Biology at the University of Siegen, Germany. He received his Dr rer. nat. degree in Analytical Chemistry (2007) from the University of Muenster, Germany, and was a postdoctoral associate at Indiana University, USA, with Prof. Gary M. Hieftje (2008–2010). His research interests include fundamentals and applications of plasma-based techniques, development of instrumentation, nanomaterial characterization, and ambient desorption/ionization.

1 Introduction

1.1 Nanomaterials

Nanotechnology is a rapidly developing field of science which utilizes materials and their properties at the nanometer (10^{-9} m) scale. The basic idea of nanotechnology has been formulated already in 1960 by Richard P. Feynman: "What would the properties of materials be if we could really arrange the atoms the way we want them?"[2] Indeed, materials at the nanometer scale possess unique properties different from those of chemically identical bulk materials. The fact that matter has distinct size-dependent properties led to the development of colloid chemistry. The first systematic studies in this field were conducted by Michael Faraday when he described the properties of "ruby" gold (Au) suspensions in 1857.[3] "The state of division of these particles must be extreme; they have not as yet been seen by any power of the microscope."[3] This statement is proof that the task of analyzing Au nanoparticles (NPs) was a challenge. The variety of states and properties of nanomaterials still presents a challenge for their characterization in analytical chemistry, even after more than 150 years after the term "colloid" was first coined.[4] The invention of electron microscopes in the 20th century has allowed scientists to visualize nanomaterials (*i.e.* particles of any shape with at least one dimension of a size between 1 nm and 100 nm). Although microscopy-based techniques became prominent nanomaterial analysis tools, they have some limitations, namely, difficult sample preparation, limited area of analysis, and measurement of projections (not three-dimensional imaging). Therefore, alternative analysis methods are needed.

An alternative method for nanomaterial characterization is single particle inductively coupled plasma mass spectrometry (spICP-MS, also referred to as SP-ICP-MS depending on the author).[5] The technique utilizes a standard ICP-MS setup, and makes use of time-resolved detection to probe NPs that are introduced into diluted suspensions (ideally) one by one. Since the first publications, the field has grown rapidly (Fig. 1) and, in the authors' estimation, will continue to grow. There have been several reviews focusing on the topic of spICP-MS,[6–9] discussing the principles, potential, limitations, and selected applications. The goal of this review is to critically discuss the latest developments and remaining challenges of spICP-MS and its metrology, to highlight instrumental parameters that are important for NP detection, and to inform the reader about the latest applications of spICP-MS when used with and without particle fractionation methods.

1.2 Principle and early development of spICP-MS

The basic principle of spICP-MS is that NPs can be detected individually if they are introduced sequentially into diluted suspensions and the detector readout frequency is sufficiently high. The constituents of a given single NP generate a discrete pulse of ions at a corresponding mass-to-charge ratio (m/z) on the order of a few hundreds of microseconds above the continuous background.[10] The signal abundance is proportional to the mass of an NP after careful calibration of the system. NP size can then be calculated from the NP mass if an element-specific density and particle geometry are assumed. The frequency of the detected signal pulses can be related to the particle number concentration (PNC) in the suspension. Overall, spICP-MS allows obtaining the average size, size distribution, and PNC of NPs after only a few minutes of measurement. Quantification and calibration strategies were summarized and described in detail in other older reviews,[6–9] so they will be discussed only shortly below.

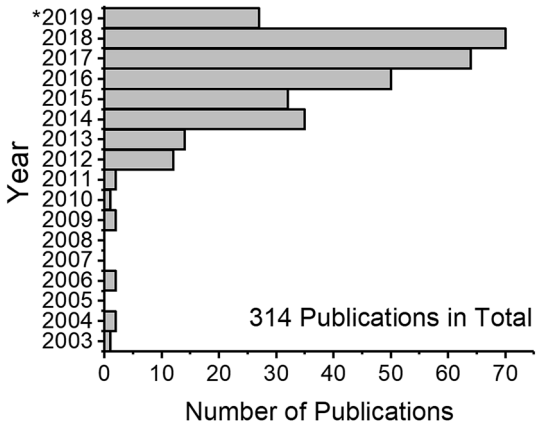

Fig. 1 Number of spICP-MS publications according to the Web of Science database (accessed on 28 May 2019). 314 publications in total. The search command: "SP-ICP-MS" or "SP-ICPMS" or "sp-ICPMS" or "single particle ICPMS" or "single particle ICP-MS" or "single particle inductively coupled plasma mass spectrometry" or "single particle inductively coupled plasma mass-spectrometry" (the characters are not register sensitive). Note that two publications published in 2004–2006, which do not use the abovementioned terms, were added manually. *The results for 2019 are incomplete.

The history of discrete particle detection has already been described.[8] The first utilization of an ICP source for time-resolved particle analysis was published by Kawaguchi *et al.*[11] In their paper, micrometer-sized particles were generated after the desolvation of monodisperse NaCl, $Ca(NO_3)_2$, and $Cu(NO_3)_2$ droplets. The method was based on optical emission spectrometry (OES) detection and intended for the analysis of particles in air. Time resolved detection of $MnCO_3$ particles in model aerosol samples with ICP-OES was reported by Bochert and Dannecker to obtain a particle size distribution.[12] Later, the group of Kawaguchi adapted the technique to ICP-MS (the commercial detector was modified) to achieve 15 times lower mass detection limits (LODs) and detect femtogram amounts of zinc.[13] This method utilized monodisperse droplets of $Zn(CH_3COO)_2$ and $Pb(NO_3)_2$ suspensions that were dried to produce particles, which were then introduced into the ICP-MS. Two years later it was shown that instrumental conditions significantly affect the resulting particle signal.[14] For example, the combination of radio frequency (RF) power, sampling position, and carrier gas (also referred to as "nebulizer gas") flow were shown to influence the signal. For Zn-containing particles, optimal conditions for particle

detection were reported to be 1400 W RF power, 14 mm sampling position, and 0.8 L min^{-1} carrier gas flow; however, no other elements or matrices were tested. At that time, the main future applications for air and aerosol analysis were predicted to be environmental studies (detection of contaminants in air) and control of clean environments (*e.g.* clean rooms in industrial application).[11,13–16] Also, the detection of particles from suspensions with ICP-OES was reported.[17,18] For example, Knight *et al.* studied micrometer-sized particles of refractory oxides and silicates.[18] They pointed out that due to incomplete droplet vaporization and particle ionization, the response obtained for 3–7 μm silica particles was not proportional to the mass of the analytes. Furthermore, the mass calibration "still has remained a problem" when the article was published, due to a lack of commercially available particles (detectable by ICP-OES) with narrow size distributions.[18]

A feasibility study for colloid suspension analysis with spICP-MS was published by Degueldre and Favarger in 2003.[5] In the paper, results of spICP-MS with 10 ms dwell time for the analysis of polydisperse 400 nm (median size) TiO_2, 150 nm Al_2O_3, 400 nm FeOOH, and some natural colloids were presented. The choice of isotopes for detection was discussed in detail because of the mass interference experienced by light elements in a single quadrupole ICP-MS (ICP-Q-MS), and $^{48}Ti^+$, $^{27}Al^+$, $^{57}Fe^+$, and $^{44}[SiO]^+$ were chosen for NP detection in a model water matrix. Similar studies were published by the same authors for 100 nm ZrO_2,[19] manually milled ThO_2 (ref. 20) and UO_2,[21] and 80 to 250 nm Au particles.[22] The studies utilized PNC of 10^5 to 10^6 cm^{-3}, and the method was presented as an alternative to microscopy investigations.[5,19–22]

After the first publications on spICP-MS between 2003 and 2011, the total number of publications first doubled in 2012 (*cf.* Fig. 1). According to a search in the Web of Science database, interest in this method is steadily growing and over 300 peer-reviewed manuscripts on the topic have been published to date. The next chapter is dedicated to the description of improvements of the spICP-MS method and areas that require further research and where the methodology can be further developed in the opinion of the authors.

2 A step towards an ideal spICP-MS method

The title and idea of the article were inspired by plenary lectures of Gary M. Hieftje[23,24] and his publication dedicated to Howard Malmstadt in 2006.[1] Howard Malmstadt's research reportedly followed the concept of an "ideal". He was known to first define the qualities of an ideal "concept, method, device, or system", and the research itself was then aimed at overcoming the identified weaknesses.[1] In the same paper,[1] the characteristics of such "an ideal method for atomic spectroscopy" were defined. These characteristics comprise, among others, the LOD of a single atom, no spectral or matrix interference, simultaneous multielement detection, and standardless analysis.[1] These ideal characteristics warrant another look here and will be compared to performance characteristics as they are related to spICP-MS and NP analysis to date. The capabilities and advances of the method along with the limitations are critically discussed and future areas of research are identified which would help to bring us closer to what would be an ideal spICP-MS method.

2.1 Sample preparation

"An ideal method for atomic spectroscopy" would require no sample preparation, and, ideally, liquid samples could be analyzed with spICP-MS without any sample preparation. In reality, this can be done only for model solutions (and not for unknown samples); however, this still requires an abundance of factors to be considered beforehand, especially when a significant amount of matrix is present, in order not to alter the state of NPs. Nanomaterials possess high surface energy that makes them more reactive compared to bulk materials of the same composition; therefore, the stability of the NP suspensions should always be considered during storage, handling, sample preservation, and sample preparation. Different dispersion media or dilutions, interactions with materials of the sampling or storage containers, storage conditions, and storage time may alter the surface coating or size of the NPs and cause aggregation. Moreover, a certain PNC range is required for analysis to measure the NPs individually. The required PNC range for analysis is discussed here in detail, as it depends on a plethora of factors (nebulization and transport efficiency, type of nebulizer and sample introduction system, elemental composition and size of the NPs *etc.*). If the samples are too diluted, measurement time can be increased to enhance the number of detected particles. In some cases, matrix interference can be reduced by sample dilution.

Nanomaterials often come in complex matrices (*e.g.* solid matrices and environmental and food samples) and require carefully optimized sample preparation protocols for their successful extraction and spICP-MS analysis. Table 1 presents an overview of all papers which report sample preparation strategies for spICP-MS sorted by the type of matrix (*e.g.* animal tissue, cell cultures, body fluids, cosmetics *etc.*) and by the publication year. This table is intended to help the reader to easily grasp the experimental details. In addition, the reader is advised that the main challenges of sample preparation are discussed in some detail in other papers and reviews.[25,26]

It is fundamentally important when using complex matrices to consider that the state of NPs may change due to filtering (NPs may interact with filter membranes), species interconversion (NPs may partially dissolve and form ionic species or ionic species can be reduced to corresponding metals), extraction and digestion procedures, or storage. At the current state of knowledge and as it is used today, spICP-MS is considered to be very suitable for the analysis of liquid samples without any sample preparation but only in the case of a rather simple matrix. In all other cases, a careful sample preparation method development is required for the analysis of complex, in particular, solid matrices to ensure that NPs do not change in their size, form, or aggregation state.

Table 1 Summary of peer-reviewed spICP-MS nanoanalysis papers with selected experimental conditions, sample matrices, and particle size LODs[a]

Year	NP types analyzed	Matrix	Sample preparation	Nebulizer and spray chamber	Plasma parameters	Mass analyzer	Measured isotopes	Dwell time	Size LOD (ESD)	Features	Ref.
Animal tissue											
2012	<20 nm NM-300K or <15 nm PVP-coated Ag NPs	Rat tissue	Enzymatic digestion with proteinase K	Babington nebulizer	RF power 1400 W	Q	$^{107}Ag^+$, $^{109}Ag^+$	3 ms	20 nm	Oral exposure of rats over a period of 28 days	104
2013	30, 80, and 1500 nm Ag NP powders, 30, 70 nm PVP-coated Ag NPs	*Lumbriculus variegatus* tissue	Sonication with water and 0.45 μm filtering	n/s	n/s	Q	n/s	n/s	n/s	NPs detected in tissue even after 48 h depuration	105
2013	100 nm PVP-coated Au NPs, 60 and 100 nm PVP-coated Ag NPs	Spiked ground beef, *Daphnia magna*, *Lumbriculus variegatus* tissues, aqueous samples	Alkaline digestion with TMAH	Glass nebulizer, cyclonic spray chamber	n/s	Q	n/s	10 ms	n/s		106
2013	Ag nanowires with PVP or aluminum doped SiO_2 coatings	*Daphnia magna* hemolymph, aqueous samples	Dilutions, where necessary	n/s	n/s	Q	$^{107}Ag^+$, $^{197}Au^+$	10 ms	<30 nm ESD		107
2014	60 nm Au NPs	Rat tissue	Alkaline TMAH digestion and enzymatic digestion with proteinase K	MicroFlow PFA nebulizer, cyclonic spray chamber	RF power 1550 W, cooling gas 14 L min^{-1}, auxiliary gas 0.8 L min^{-1}, nebulizer gas 0.96–0.99 L min^{-1}	Q	$^{197}Au^+$	3 ms	Only NPs >44 nm were considered	Intravenous administration of the NPs	108
2014	60 nm citrate-coated Ag NPs	Spiked chicken meat	Enzymatic digestion with proteinase K	Conical glass concentric nebulizer, quartz impact bead spray chamber	RF power 1400 W, cooling gas 13 L min^{-1}, auxiliary gas 0.7 L min^{-1}, nebulizer gas 1.1 L min^{-1}	Q	$^{107}Ag^+$	3 ms	n/s		109
2014	<25 nm anatase TiO_2	Rat spleen	Enzymatic digestion with proteinase K	PFA micronebulizer, heated cyclonic spray chamber, desolvation system	n/s	Q	$^{49}Ti^+$	3 ms	n/s	Oral exposure	110
2015	50 nm PVP-coated Ag NPs	Earthworm tissue	Enzymatic digestion with proteinase K	Conical glass concentric nebulizer, quartz impact bead spray chamber	RF power 1400 W, cooling gas 13 L min^{-1}, auxiliary gas 0.7 L min^{-1}, nebulizer gas 1.1 L min^{-1}	Q	$^{107}Ag^+$	3 ms	30 nm	*In vivo* exposure in soil	111

Table 1 (*Contd.*)

Year	NP types analyzed	Matrix	Sample preparation	Nebulizer and spray chamber	Plasma parameters	Mass analyzer	Measured isotopes	Dwell time	Size LOD (ESD)	Features	Ref.
2015	42 nm PVP-coated Ag NPs	Spiked chicken meat	Reference to previous studies	Reference to previous studies	Reference to previous studies	n/s	n/s	n/s	n/s	Two laboratories carried out the analysis with different methods	112
2017	18–20 nm Ag NPs	Mouse maternal tissues, placentas, foetuses	Alkaline digestion with TMAH	Quartz concentric nebulizer, cyclonic spray chamber	n/s	Q	$^{107}Ag^{+}$	0.1 ms	13 nm	Nose-only inhalation of a NP aerosol for pregnant female mice	113
2017	20 nm PVP-coated Ag NPs	Hen livers and yolks	Enzymatic digestion with proteinase K	n/s	RF power 1000 W, cooling gas 15 L min^{-1}, auxiliary gas 1.2 L min^{-1}, nebulizer gas 1.1 L min^{-1}	SF mass analyzer was used in low resolution mode	$^{109}Ag^{+}$	2 ms	10 nm	Oral administration to hens	114
2017	30 and 60 nm Au NPs	*Caenorhabditis elegans* nematode	Alkaline digestion with TMAH	C-type nebulizer, impact bead spray chamber	n/s	Q	$^{197}Au^{+}$	10 ms	n/s	Sucrose density gradient centrifugation was used to remove non-ingested NPs	115
2017	40 to 750 nm Pb NPs	Game meat	Enzymatic digestion with proteinase K	Low-flow concentric nebulizer, cyclonic spray chamber	RF power 1550 W, cooling gas 14 L min^{-1}, auxiliary gas 0.65 L min^{-1}, nebulizer gas 1.10 L min^{-1}	Q	$^{208}Pb^{+}$	5 ms	40 to 80 nm	Lead from bullets; size LOD was reported to depend on the lead background	116
2017	26 nm Ag NPs	Chicken meat paste after *in vitro* model, saliva, gastric, and intestinal digestions	Dilution of digest extracts	MicroMist nebulizer, Scott-type spray chamber	RF power 1500 W, cooling gas 15 L min^{-1}, auxiliary gas 0.73 L min^{-1}, nebulizer gas 0.68 L min^{-1} (these conditions specified only for total silver analysis)	Q	$^{107}Ag^{+}$	10 ms	n/s		117
2017	15 to 75 nm PVP-coated Ag NPs	Spiked chicken muscle meat	Enzymatic digestion with proteinase K	Varied among the participants	Varied among the participants	Q or n/s	n/s	3 ms	15–20 nm	Interlaboratory method performance study with over 10 laboratories	82

Table 1 (*Contd.*)

Year	NP types analyzed	Matrix	Sample preparation	Nebulizer and spray chamber	Plasma parameters	Mass analyzer	Measured isotopes	Dwell time	Size LOD (ESD)	Features	Ref.
2017	60 and 80 nm Au NPs	LA-SP-ICP-MS imaging of mice heart, lung, spleen, liver, kidney	Intravenous injection	n/s	RF power 1400 W, nebulizer gas 0.7 L min^{-1}	Q	$^{197}Au^{+}$	0.1 ms	n/s		118
2018	CeO_2 NPs	Liver and lung tissue of female mice	Enzymatic digestion with proteinase K	Low-flow concentric nebulizer, cyclonic spray chamber	RF power 1550 W, cooling gas 14 L min^{-1}, auxiliary gas 0.8 L min^{-1}, nebulizer gas 1.1 L min^{-1}	Q	$^{140}Ce^{+}$	3 ms	18 nm	Intravenous injection of NPs; no NPs in liver were detected after oral exposure	119
2018	30 and 80 nm PVP-coated Ag and Au NPs	Liver, gill, and intestine tissue of zebrafish (*Danio rerio*), aqueous samples	Alkaline digestion with TMAH	n/s	RF power 1550 W, nebulizer gas 1.14 L min^{-1}, sampling position 8.0 mm	Q	$^{107}Ag^{+}$, $^{197}Au^{+}$	0.1 ms	n/s		120
2018	50 and 100 nm rutile TiO_2 NPs	*Bivalve mollusk*	Ultrasound assisted enzymatic digestion with a pancreatin and lipase mixture	Glass concentric or PFA nebulizer (n/s clearly), cyclonic spray chamber	RF power 1600 W, cooling gas 16 L min^{-1}, auxiliary gas 1.2 L min^{-1}, nebulizer gas 0.95 L min^{-1}	Q	$^{49}Ti^{+}$	0.1 ms	24.4–30.4 nm		121
2018	TiO_2 and CeO_2 NPs	Spiked zebrafish (*Danio rerio*) (intestine, liver, gills, and brain)	Enzymatic digestion with proteinase K, H_2O_2 treatment, SDS stabilization	Conical glass nebulizer, impact bead spray chamber	RF power 1400 W, cooling gas 13 L min^{-1}, auxiliary gas 0.7 L min^{-1}, nebulizer gas 1.1 L min^{-1}	Q	$^{48}Ti^{+}$, $^{140}Ce^{+}$	3 ms	100 nm TiO_2, 30–40 nm CeO_2	Method for NP extraction from tissue was optimized	122
Biological applications											
2009	20, 40, and 80 nm Au NPs	Immunoassay with NPs as tags to antibodies	2% HNO_3 to release the tags, dilution	Glass concentric nebulizer, impact bead spray chamber	RF power 1400 W, cooling gas 13 L min^{-1}, auxiliary gas 0.8 L min^{-1}, nebulizer gas 0.85 L min^{-1}	Q	$^{197}Au^{+}$	10 ms	15 nm		123
2014	25 nm Au, 25 nm Ag, and 20 nm Pt citrate-coated NPs	Multiplex DNA assay with NP tags	Melting wash, dilution	n/s	RF power 1200 W, cooling gas 13 L min^{-1}, auxiliary gas 0.8 L min^{-1}, nebulizer gas 0.82 L min^{-1}	Q	$^{107}Ag^{+}$, $^{197}Au^{+}$, $^{195}Pt^{+}$	0.5 ms			124
2015	80 nm citrate-coated Au NPs	Primary human umbilical vein endothelial cells	Alkaline digestion with TMAH	MicroFlow PFA nebulizer, cyclonic spray chamber	RF power 1550 W, cooling gas 14 L min^{-1}, auxiliary gas 0.8 L min^{-1},	Q	$^{197}Au^{+}$	10 ms	n/s		125

Table 1 (*Contd.*)

Year	NP types analyzed	Matrix	Sample preparation	Nebulizer and spray chamber	Plasma parameters	Mass analyzer	Measured isotopes	Dwell time	Size LOD (ESD)	Features	Ref.
					nebulizer gas 0.96–0.99 L min^{-1}						
2016	7 and 20 nm TiO_2 NPs; 50 and 75 nm citrate-coated Ag NPs	Mouse neuroblastoma cells	Lysis in Triton X-100	n/s	RF power 1400 W, additional gas flow (Ar) 0.95 L min^{-1}	Q	$^{107}Ag^+$, $^{48}Ti^+$	3 ms	22 nm Ag, 69 nm TiO_2		126
2016	10, 30, and 70 nm PEG-BPEI-, and citrate-coated Ag NPs	OECD 201 culture medium with *Pseudokirchiniella subcapitata*	Filtration (0.45 μm pore size), dilution	n/s	n/s	TQ	$^{107}Ag^+$	3 ms	n/s		127
2018	18 nm Al NPs, 20 nm Al_2O_3 NPs, 25 nm TiO_2 NPs	Model cell culture medium	n/s	PFA nebulizer, cyclonic spray chamber	Cooling gas 13 L min^{-1}, auxiliary gas 0.7 L min^{-1}, nebulizer gas 0.89 L min^{-1}	Q	n/s	3 ms	54 nm Al, 50 nm Al_2O_3, 60–100 nm TiO_2	Several methods for NP characterization are described	128
2018	NPs formed from Cr^{III} salts	Medium for algal ecotoxicity testing	Dilution	MicroMist nebulizer	RF power 1500 W, cooling gas 13.5 L min^{-1}, auxiliary gas 0.77 L min^{-1}, nebulizer gas 0.87 L min^{-1}	Q	$^{52}Cr^+$	0.05 ms	90 nm $Cr(OH)_3$		129
2019	30 nm citrate-coated Au NPs	Oligonucleotide-functionalized Au NPs after sandwich hybridization reaction-capture	See article for detailed procedure	Glass concentric nebulizer, impact bead spray chamber	RF power 1750 W, cooling gas 17 L min^{-1}, auxiliary gas 1 L min^{-1}, nebulizer gas 1.05 L min^{-1}	Q	$^{197}Au^+$	3 ms	n/s		130
Body fluids and tissue											
2012	60 nm citrate-coated Ag NPs	Model saliva, gastric, duodenal, and bile juices with and without proteins	Dilution	Babington type nebulizer, impact bead spray chamber	RF power 1400 W, cooling gas 13 L min^{-1}, auxiliary gas 0.7 L min^{-1}, nebulizer gas 1.1 L min^{-1}	Q	$^{107}Ag^+$	n/s	n/s		131
2015	44.5 ± 9.2 nm citrate-coated Au NPs	Spiked whole blood of rats	Dilution	MicroMist glass nebulizer	Nebulizer gas 1.05 L min^{-1}	Q	$^{197}Au^+$	10 ms	n/s		132
2017	Respirable crystalline silica	Exhaled breath condensate		n/s	n/s	Q with KED (He)	$^{28}Si^+$	3 ms	300 nm		133
2017	10, 30, 50, 60, 80, and 100 nm citrate- or carboxylic acid-	Spiked human whole blood	Dilution with Triton X, TMAH, and water	Concentric glass nebulizer, conical spray chamber	Nebulizer gas 1.06 L min^{-1}	Q	$^{107}Ag^+$, $^{197}Au^+$	0.05 ms	30 nm		134

Table 1 (*Contd.*)

Year	NP types analyzed	Matrix	Sample preparation	Nebulizer and spray chamber	Plasma parameters	Mass analyzer	Measured isotopes	Dwell time	Size LOD (ESD)	Features	Ref.
	coated Ag and Au NPs										
2018	40 nm PEG-coated Ag NPs, broadly distributed PEG-, sodium carboxylate-coated Ag NPs	Spiked human placental tissue	Alkaline digestion with TMAH, enzymatic digestion with proteinase K	MicroMist nebulizer, Scott spray chamber	RF power 1550 W, cooling gas 15 L min^{-1}, nebulizer gas 1.03 L min^{-1}	TQ	$^{107}Ag^{+}$	3 ms	25 nm		135
2018	Broadly distributed PEG-, sodium carboxylate-coated Ag NPs	Human *ex vivo* placenta perfusion model	Enzymatic digestion with proteinase K	MicroMist nebulizer, Scott spray chamber for TQ; MicroFlow PFA nebulizer, cyclonic spray chamber for Q	RF power 1550 W, cooling gas 15 L min^{-1}, nebulizer gas 1.03–1.05 L min^{-1}	Q, TQ	$^{107}Ag^{+}$	3 ms	25 nm		136
2019	20 nm citrate-coated Au NPs	Water, RPMI 1640 culture medium, cell and exosome lysates	Dilution, sonication	PFA-ST nebulizer	RF power 1500 W	Q	$^{197}Au^{+}$	5 ms	10 nm		137
Carbon nanotubes (CNTs)											
2013	Intercalated Co and Y NPs	Single walled CNT dispersions	Dilution of dispersed CNTs	n/s	n/s	Q	$^{89}Y^{+}$, $^{59}Co^{+}$	10 ms	n/s	Detection of trace catalytic metals intercalated in the CNTs	138
2016	Intercalated Y	Single walled CNT dispersions, *Daphnia magna* in nanopure water after CNT exposure	Dilution and sonication for *Daphnia magna* samples	n/s	RF power 1600 W, cooling gas 16 L min^{-1}, auxiliary gas 1.02 L min^{-1}, nebulizer gas 0.85–1 L min^{-1}	Q	$^{89}Y^{+}$	0.1, 10 ms	n/s		139
2017	Intercalated Y	Single walled CNTs, release supernatants containing degradation products	Surfactant addition, sonication, dilution	n/s	n/s	Q	$^{89}Y^{+}$	0.1 ms	n/s	CNT fragments were released due to photodegradation of CNTs and polycaprolactone nanocomposite	140
Cosmetics											
2015	32 to 40 nm TiO_2 NPs	Sunscreens	Dispersion in Triton X-100, dilution	Cyclonic spray chamber, Meinhard nebulizer	RF power 1600 W, nebulizer gas 1.06–1.08 L min^{-1}	Q	$^{48}Ti^{+}$	0.1 ms	27–29 nm		141

Table 1 (*Contd.*)

Year	NP types analyzed	Matrix	Sample preparation	Nebulizer and spray chamber	Plasma parameters	Mass analyzer	Measured isotopes	Dwell time	Size LOD (ESD)	Features	Ref.
2017	30 to 120 nm TiO_2 NPs	Cosmetics and personal care products	Defatting with hexane, suspension in water, dilution or suspension in SDS, dilution	Cyclonic spray chamber, Meinhard nebulizer	RF power 1450 W	Q	$^{48}Ti^+$, $^{197}Au^+$	0.1 ms	35 nm TiO_2	No Au NPs were found in the tested samples	142
2018	≤107 nm TiO_2 and ≤98 nm ZnO NPs	Cream and spray sunscreens	Dispersion in Triton X-100, dilution	PFA nebulizer	n/s	Q with KED (He)	$^{48}Ti^+$, $^{64}Zn^+$	5 ms	25 nm TiO_2, 50 nm ZnO		143
2018	TiO_2 NPs	Sunscreen, coating of chocolate candies	Defatting with hexane, filtration, dilution for sunscreen; extraction with water, sonication, filtration, dilution for coating	Meinhard nebulizer, cyclonic spray chamber	n/s	Q	$^{48}Ti^+$	0.1 ms	32 nm		144
2018	TiO_2 and ZnO NPs	Sunscreen powder	Dispersion in Triton X-100, dilution	n/s	n/s	n/s	n/s	n/s	n/s		145
2018	Al_2O_3, TiO_2, SiO_2 NPs	AF4 fractions after toothpaste fractionation	Dilution, see the article for detailed sample preparation procedure	Low-flow concentric nebulizer, cyclonic spray chamber	RF power 1549 W, cooling gas 14 L min^{-1}, auxiliary gas 0.79 L min^{-1}, nebulizer gas 1.04 L min^{-1}	Q	$^{27}Al^+$, $^{47}Ti^+$	10 ms	55–65 nm Al_2O_3 and TiO_2 NPs		146
Model environmental aqueous samples											
2013	Nanoparticulate Zn, Mo, and Ag in leachates	Model freshwater, seawater, acidic rainwater	Leaching	n/s	RF power 1550 W, cooling gas 15 L min^{-1}, auxiliary gas 0.35 L min^{-1}, nebulizer gas 0.79 L min^{-1}	Q with KED (He)	$^{66}Zn^+$, $^{98}Mo^+$, $^{107}Ag^+$	30 ms	n/s	Leaching of CIGS and OPV cells into model water was studied	147
2014	50 nm PVP-coated Ag NPs	Spiked littoral mesocosms on a lake	Spiking, dilution	n/s	n/s	Q	$^{107}Ag^+$	10 ms	30 nm		148
2014	60 and 100 nm citrate-, tannic acid-, and PVP-coated Ag NPs	Spiked deionized, tap, surface, and EPA moderately hard reconstituted laboratory water	Spiking	n/s	n/s	Q	$^{107}Ag^+$	10 ms	25–30 nm	NP dissolution kinetic study	149

Table 1 (*Contd.*)

Year	NP types analyzed	Matrix	Sample preparation	Nebulizer and spray chamber	Plasma parameters	Mass analyzer	Measured isotopes	Dwell time	Size LOD (ESD)	Features	Ref.
2014	50 nm citrate-coated and 80 nm PVP-coated Ag NPs	Spiked purified water, waste water influent and effluent, river water	Filtration (0.45 μm pore size), spiking	Glass conical nebulizer, conical spray chamber with impact bead	RF power 1450 W, cooling gas 15 L min^{-1}, nebulizer gas 0.85 and 0.93 L min^{-1}	Q	$^{107}Ag^{+}$, $^{109}Ag^{+}$	5 ms	40 nm	Internal calibration with isotope dilution (^{109}Ag enriched silver standard) was used, both silver isotopes were monitored in one run with 1.9 ms settling time	66
2016	80–200 nm ZnO NPs, 30–50 nm CeO_2 NPs, Zn- and Ce-containing NPs	Spiked river water after real and model drinking water treatment, river water	Spiking, water treatment, dilution or no treatment	Meinhard concentric nebulizer, cyclonic spray chamber	RF power 1600 W, cooling gas 18 L min^{-1}, auxiliary gas 1.2 L min^{-1}, nebulizer gas 1.02–1.06 L min^{-1}	Q	$^{67}Zn^{+}$, $^{140}Ce^{+}$	0.1 ms	35–40 nm ZnO, 18–20 nm CeO_2		150
2016	Ti-containing NPs; 100 and 160 nm TiO_2 NPs; 40, 70, and 100 nm citrate-coated Ag NPs; 50, 80, and 100 nm citrate-coated Au NPs	Spiked river water after real and model drinking water treatment, river water	Spiking, water treatment, dilution or no treatment	Meinhard concentric nebulizer, cyclonic spray chamber	RF power 1600 W, cooling gas 18 L min^{-1}, auxiliary gas 1.2 L min^{-1}, nebulizer gas 1.02–1.06 L min^{-1}	Q	$^{47}Ti^{+}$, $^{197}Au^{+}$, $^{107}Ag^{+}$	0.1 ms	65–70 nm TiO_2, 21–23 nm Ag, 27–30 nm Au		151
2016	80 nm citrate- and PVP-coated Ag NPs	Spiked waste water effluent and mixed liquor	Filtration (0.45 μm pore size), spiking	Concentric glass nebulizer, cyclonic spray chamber	RF power 1600 W	Q	$^{107}Ag^{+}$	0.1 ms, 10 ms	10 nm for double deionized water		152
2016	20 and 50 nm citrate-, PVP-, and lipoic acid-coated Ag NPs	Spiked lake water	Filtration (0.22 μm pore size), spiking	n/s	RF power 1550 W, cooling gas 15 L min^{-1}	Q	$^{107}Ag^{+}$, $^{109}Ag^{+}$	5 ms	24 nm		153
2016	30, 60, 80, and 100 nm tannic acid-coated Au NPs	Spiked river and waste water	Filtration (0.45 μm pore size), spiking	MicroMist nebulizer	RF power 1550 W, auxiliary gas 0.1 L min^{-1}, nebulizer gas 1.05 L min^{-1}	Q	$^{197}Au^{+}$	3 ms	19 nm for ultrapure water, 31 nm for 0.1 μg L^{-1} Au^{3+}		154
2016	75 nm PVP-coated Ag NPs	Reaction in aerated, sulfide-containing water and EPA moderately hard reconstituted water standard	Spiking, dilution	Microflow concentric PFA nebulizer, impact bead spray chamber	n/s	Q	$^{107}Ag^{+}$	10 ms	15 nm		155

Table 1 (*Contd.*)

Year	NP types analyzed	Matrix	Sample preparation	Nebulizer and spray chamber	Plasma parameters	Mass analyzer	Measured isotopes	Dwell time	Size LOD (ESD)	Features	Ref.
2016	40 and 80 nm citrate-coated Ag NPs	Spiked waste water effluent and influent, river water	Filtration (0.45 μm pore size), spiking, HDC	Concentric nebulizer	n/s	Q	$^{107}Ag^{+}$	0.1 ms	24 nm		102
2016	50 and 80 nm citrate- or PVP-coated Ag NPs	Spiked MilliQ water, chloride containing MilliQ water, MilliQ water at pH 5, 7, and 7.6	Spiking	Conical nebulizer, impact bead spray chamber	RF power 1450 W, cooling gas 15 L min^{-1}, nebulizer gas 0.85 L min^{-1}	Q	$^{107}Ag^{+}$	5 ms	40 nm without Ag^{+}	Ozonation was used for selected samples	156
2017	50 nm citrate- and tannic acid-coated Ag NPs	Spiked waste water effluent, MilliQ water, modified TAP medium	Spiking, dilution, IEC	n/s	n/s	Q	n/s	0.5 ms	17 nm		157
2017	10, 20, 30, 40, 50, 60, 70, 80, and 100 nm PVP-coated Ag NPs	Spiked lake and tap water, liquid consumer products, migration solutions from plasters	Spiking, dilution	Cyclonic spray chamber, Meinhard concentric nebulizer	n/s	Q	$^{107}Ag^{+}$	0.05 ms	12–15 nm		158
2017	20, 40, 80, 100, and 200 nm PVP-coated and commercial Ag NPs	Spiked waste water effluent, environmental water	Spiking, centrifugation	n/s	n/s	Q	n/s	10 ms	n/s		159
2017	10–25 nm TiO_2 and 10–30 nm ZnO NPs	Spiked river water	Spiking, dilution	Reference to previous studies	Reference to previous studies	Q	$^{47}Ti^{+}$, $^{66}Zn^{+}$	0.1 ms	64 nm TiO_2, 43 nm ZnO		160
2017	30–50 nm PVP-coated Ag NPs	Spiked MilliQ and lake water with gum arabic	Sonication, dilution	n/s	n/s	Q	$^{107}Ag^{+}$	5 ms	40 nm		161
2017	60 nm Ag–Ag core–shell NPs (30 nm core, 15 nm shell)	Spiked EPA moderately hard water with or without fulvic acid	Spiking	Cyclonic spray chamber, Meinhard concentric nebulizer	RF power 1600 W	Q	$^{107}Ag^{+}$, $^{197}Au^{+}$	0.1 ms	15.5 nm Ag		162
2017	40, 80, and 100 nm citrate- or PVP-coated Ag NPs	Spiked wastewater biosolids (raw or supernatant)	Filtration (0.45 μm pore size), spiking	Cyclonic spray chamber, type C0.5 concentric glass nebulizer	n/s	Q	$^{107}Ag^{+}$	0.5 ms	n/s		163
2017	40 and 60 nm BPEI- and PVP-coated Ag NPs	Spiked microcosm tanks with seawater	Spiking	Flow injection, pneumatic nebulizer	Reference to previous studies	Q	$^{107}Ag^{+}$	10 ms	n/s		164

Table 1 (*Contd.*)

Year	NP types analyzed	Matrix	Sample preparation	Nebulizer and spray chamber	Plasma parameters	Mass analyzer	Measured isotopes	Dwell time	Size LOD (ESD)	Features	Ref.
2017	40 nm citrate-coated Ag NPs	Spiked WWTP mesocosm	Filtration (0.1 mm pore size), spiking	Cyclonic spray chamber, Burgener Mira Mist nebulizer	RF power 1205 W, cooling gas 15.01 L min^{-1}, auxiliary gas 0.75 L min^{-1}, nebulizer gas 0.520 L min^{-1}	SF	n/s	0.1 ms	From 5.4 nm to 30–40 nm		62
2018	Aged 34 nm citrate-coated Ag NPs, Ag-containing aggregates	Remobilization medium (remobilization from a model sediment)	Dilution, filtration (1 μm pore size) or no filtration	n/s	n/s	Q	$^{107}Ag^{+}$	5 ms	30 nm		165
2018	40, 70, and 100 nm citrate-coated Ag; 50, 80, and 100 nm citrate-coated Au; 100 nm TiO_2; 30–50 nm CeO_2; 80–200 nm ZnO NPs	Spiked river and lake water with alum, ferric oxides, or ferric sulfate	Dilution	Reference to previous studies	Reference to previous studies	Q	$^{47}Ti^{+}$	0.1 ms	25 nm Ag, 30 nm Au, 70 nm TiO_2, 23 nm CeO_2, 44 nm ZnO		166
2018	25 nm PVP-coated Ag NPs, 5 nm TiO_2 NPs	Effluent of a lab-scale WWTP	Sonication, dilution	n/s	n/s	Q	$^{107}Ag^{+}$	3 ms	n/s		167
2018	30, 50, 80, and 100 nm citrate-coated and 60 and 100 nm PVP-coated Ag NPs	Spiked tap, river water, waste water influent	Spiking, Ag^{+} was adsorbed by magnetic reduced graphene oxide	n/s	RF power 1550 W, cooling gas 15 L min^{-1}	Q	$^{107}Ag^{+}$	3 ms	20 nm		168
2018	30–50 nm PVP-coated Ag NPs	Spiked surface water of a boreal oligotrophic lake	Lake spiking	Reference to previous studies	Reference to previous studies	SF	$^{107}Ag^{+}$	0.05 ms	12 nm		169
2018	30–50 nm PVP-coated Ag NPs	Spiked surface water of a boreal oligotrophic lake	Lake spiking	Glass conical nebulizer	RF power 1450 W, cooling gas 15 L min^{-1}	Q	$^{107}Ag^{+}$	5 ms	45 ± 5 nm		170
2018	50 nm zero-valent iron NPs, Cd^{2+} sorbed to the NPs	Spiked Milli-Q water, synthetic and effluent waste water	Spiking, shaking	Scott spray chamber	RF power 1550 W, cooling gas 15.0 L min^{-1}, auxiliary gas 0.90 L min^{-1}, nebulizer gas 1.09 L min^{-1}, sampling position 8 mm	TQ	$^{56}Fe^{+}$, $^{111}Cd^{+}$	3 ms	36 nm	H_2 was used as a reaction gas	171

Table 1 (*Contd.*)

Year	NP types analyzed	Matrix	Sample preparation	Nebulizer and spray chamber	Plasma parameters	Mass analyzer	Measured isotopes	Dwell time	Size LOD (ESD)	Features	Ref.
2019	20,40, and 60 nm citrate-coated Ag NPs	Spiked Milli-Q water, spiked wastewater	CPE	PFA microflow nebulizer, cyclonic spray chamber	RF power 1600 W, cooling gas 18.0 L min^{-1}, auxiliary gas 1.2 L min^{-1}, nebulizer gas 0.83 L min^{-1}	Q	$^{107}Ag^{+}$	0.1 ms	>20 nm	Optimization of CPE was performed	172
Environmental aqueous samples											
2014	TiO_2 NPs released from sunscreen products	Suspended particulate matter of old Danube Lake, Vienna, Austria	Dilution	n/s	n/s	Q	$^{47}Ti^{+}$	10 ms	130 nm	Interference of $^{48}Ti^{+}$ with $^{48}Ca^{+}$	173
2015	50 nm ZnO NPs and Zn-containing NPs	Spiked and unspiked surface water, effluent waste water (Des Prairies River, Montreal WWTP, Canada)	Spiking, dilution or IEC (Chelex 100)	Type C0.5 concentric glass nebulizer, cyclonic spray chamber	n/s	Q	n/s	0.5 ms	32 nm for Milli-Q water, 70 nm for river water, 126 nm for waste water		174
2016	Ag-containing NPs	WWTP and surface water from the River Isar, Germany; pre-alpine lake water, Germany	CPE, dilution	n/s	n/s	Q	$^{107}Ag^{+}$	3 ms	14 nm		175
2016	Citrate-coated Ag NPs, tannic acid-coated Au NPs, Ag- and Au-containing NPs	Spiked filtered natural and waste water, unspiked natural water (Guiyu and Xiangjiang Rivers and Chendian Lake, China) and waste water (HuNan University, China)	Filtration with a nylon membrane (0.45 and 0.22 μm pore size) before spiking; dilution for unspiked samples	MicroMist nebulizer	RF power 1550 W, auxiliary gas 0.1 L min^{-1}, nebulizer gas 1.05 L min^{-1}, sampling position 8 mm	Q	$^{107}Ag^{+}$, $^{197}Au^{+}$	3 ms	20 nm Ag, 19 nm Au		103
2017	71 and 145 nm TiO_2 NPs	Influent sewage, aeration tank contents of a WWTP (Hyderabad, India)	Microwave digestion (HNO_3 and H_2O_2), filtration with a cellulose acetate membrane (0.22 μm pore size), sonication	n/s	RF power 1550 W, nebulizer gas 1.05 L min^{-1}	n/s	$^{47}Ti^{+}$	3 and 10 ms	n/s		176
2017	Ti-containing NPs	Surface water of clear Creek in Golden, Colorado, USA	n/s	n/s	n/s	Q, SF	$^{49}Ti^{+}$ at quadrupole, $^{48}Ti^{+}$ at SF	3 ms	79 nm TiO_2 for Q, 42 nm TiO_2 for SF	SF measurements were presented as a proof of concept	177

Table 1 (*Contd.*)

Year	NP types analyzed	Matrix	Sample preparation	Nebulizer and spray chamber	Plasma parameters	Mass analyzer	Measured isotopes	Dwell time	Size LOD (ESD)	Features	Ref.
2018	Ti-containing natural NPs and engineered TiO_2 NPs	Water samples from old Danube Lake, Vienna, Austria	Sonication, centrifugation for TQ; sonication, dialysis for TOF	n/s	n/s	TQ, TOF	$^{63}TiNH^+$ for TQ, MA for TOF	4 ms for TQ, 3 ms for TOF	81 nm TiO_2 for TQ	NH_3 and He were used as reaction/collision gases	73
2018	Ag-containing NPs	Water from Vltava, Prague, Czech Republic	1% (w/w) gelatin for stabilization	PTFE concentric nebulizer, cyclonic spray chamber	RF power 1100 W, cooling gas 11 L min^{-1}, auxiliary gas 1.0 L min^{-1}, nebulizer gas 0.85 L min^{-1}	Q	$^{107}Ag^+$	0.1 ms	15 nm		178
2018	Ag-containing NPs	Bottom sediments and labile sediments from Lake Ontario, Canada, freeze-dried samples	Sonication with water, centrifugation, filtration (0.45 μm pore size)	Reference to previous studies	Reference to previous studies	SF mass analyzer was used in low resolution mode	$^{107}Ag^+$	0.05 ms	16 nm		179
2018	Ag, CeO_2, and TiO_2 NPs	Surface water of the Meuse and Ijssel Rivers, The Netherlands	Sonication	MicroFlow PFA nebulizer, cyclonic spray chamber	RF power 1550 W, cooling gas 14 L min^{-1}, auxiliary gas 0.8 L min^{-1}, nebulizer gas 1.1 L min^{-1}	Q	$^{107}Ag^+$, $^{140}Ce^+$, $^{48}Ti^+$, $^{139}La^+$	3 ms	14 nm Ag, 10 nm CeO_2, 100 nm TiO_2	MA was used with 100 μs dwell time to detect $^{140}Ce^+$ and $^{139}La^+$	180
2018	Ti-containing NPs	Water from the Salt River, pools, Arizona, USA	Filtration (0.7 μm pore size)	n/s	n/s	Q	$^{49}Ti^+$	10 ms	148 ± 3 nm for river water, 173 ± 15 nm for pool water		181
2018	Ag-containing NPs	Water from Lake Königssee and Lake Waginger see, Bavaria, Germany	CPE, dilution	n/s	n/s	Q	$^{107}Ag^+$	0.1 ms	10 nm		182
2018	Pb-, Fe-, Sn-, Cu-, Ag-, and Ti-containing particles	Tap water from Phoenix, Arizona, USA		n/s	n/s	Q with KED for $^{56}Fe^+$	$^{208}Pb^+$, $^{56}Fe^+$, $^{118}Sn^+$, $^{107}Ag^+$, $^{65}Cu^+$, $^{49}Ti^+$	10 ms	11.3 nm Pb, 55 nm Fe, 26 nm Sn, 40 nm Cu, 75 nm Ti, 13 nm Ag	No Ti- and Ag-containing NPs were discovered	183
2019	Engineered TiO_2 NPs	Sanitary sewage spills	Tetrasodium pyrophosphate treatment, stirring, sonication, centrifugation, dilution	n/s	n/s	TOF	$^{48}Ti^+$, MA	33 kHz	40 nm TiO_2	Split-particle events were summed up	184

Table 1 (*Contd.*)

Year	NP types analyzed	Matrix	Sample preparation	Nebulizer and spray chamber	Plasma parameters	Mass analyzer	Measured isotopes	Dwell time	Size LOD (ESD)	Features	Ref.
Model food samples											
2014	20, 40, and 100 nm PVP-coated Ag NPs	Food simulants (distilled water and 10% ethanol)	Dilution	Varied among the participants	Varied among the participants	n/s	n/s	3 ms	Varied among the participants	Interlaboratory method performance study with over 23 laboratories	83
2014	30 and 60 nm citrate-coated Au NPs, 60 nm citrate-coated Ag NPs	Spiked Milli-Q water, chicken digest (enzymatic digestion)	Dilution	Varied among the participants	Varied among the participants	n/s	$^{107}Ag^{+}$, $^{197}Au^{+}$	3 ms	Varied among the participants	Interlaboratory method performance study with over 9 laboratories, 3 of which used SP-ICP-MS	185
2016	60 nm PVP-coated Ag NPs	Food simulants (water, 10% ethanol, and 3% acetic acid)	Dilution	MicroMist nebulizer	RF power 1550 W, cooling gas 15 L min^{-1}	Q	$^{107}Ag^{+}$	3 ms	n/s		186
2016	10, 30, 50, 60, and 100 nm Ag NPs, 10, 20, 30, 50, 60, 70, and 80 nm Au NPs	Spiked water, orange juice, apple juice	Dilution	n/s	n/s	Q	$^{107}Ag^{+}$, $^{197}Au^{+}$	0.05 ms	31–34 nm	The coatings were not specified for each size of the NPs. Citrate-, PVP-coated Ag NPs, citrate-, carboxylic acid-coated, and PBS-buffered Au NPs were used	187
2018	40 nm PEG-, citrate-coated Ag NPs	Food simulants (10%, 20%, and 50% ethanol; 3% acetic acid; olive oil), low fat cow milk, 2% NaCl	Dilution, Triton X-100 was used to create an olive oil emulsion in water	Low-flow concentric nebulizer, cyclonic spray chamber	RF power 1550 W, cooling gas 14 L min^{-1}, auxiliary gas 0.80 L min^{-1}, nebulizer gas 0.96 L min^{-1}	Q	$^{107}Ag^{+}$	3 ms	10–20 nm		188
Food											
2014	TiO_2 NPs	Food grade TiO_2 (E171), food and personal care products	Food grade TiO_2 suspension in BSA, heating with H_2O_2 and resuspension in BSA for other products	Conical glass concentric nebulizer	RF power 1400 W	Q	$^{48}Ti^{+}$	3 ms	50 nm		189
2015	Ag NPs	Decoration of pastry (“pearls”)	Dissolution in water, dilution	MicroMist nebulizer	n/s	Q	$^{107}Ag^{+}$	3 ms	13 nm		190

Table 1 (*Contd.*)

Year	NP types analyzed	Matrix	Sample preparation	Nebulizer and spray chamber	Plasma parameters	Mass analyzer	Measured isotopes	Dwell time	Size LOD (ESD)	Features	Ref.
2018	TiO_2 NPs	Candy products	Sonication in water, dilution	MicroMist nebulizer, cyclonic spray chamber	RF power 1550 W, cooling gas 14 L min^{-1}, auxiliary gas 0.8 L min^{-1}, nebulizer gas 1.03 L min^{-1}	TQ	$^{48}Ti^+$ with O_2 gas had the highest sensitivity	10 ms	26 nm	Optimization of TQ detection was performed with different gases	57
2018	TiO_2, Cu, and Ag NPs	Drinks and food	Sample preparation varied depending on the product	Meinhard nebulizer, cyclonic spray chamber	n/s	Q	$^{107}Ag^+$, $^{63}Cu^+$, $^{48}Ti^+$	0.1 ms	32 nm TiO_2, 30 nm Ag		191
2018	Al-containing NPs	Chinese noodles	Enzymatic digestion with α-amylase	Low–low concentric nebulizer, cyclonic spray chamber	RF power 1550 W, cooling gas 13.9 L min^{-1}, auxiliary gas 0.79 L min^{-1}, nebulizer gas 1.07 L min^{-1}	Q	$^{27}Al^+$	3 ms	54–83 nm Al_2O_3		192
2019	TiO_2 NPs	Surimi (crab sticks)	Enzymatic digestion with pancreatin and lipase, dilution with 1% glycerol, sonication	n/s	RF power 1600 W, cooling gas 16 L min^{-1}, auxiliary gas 1.2 L min^{-1}, nebulizer gas 0.95 L min^{-1}	Q	$^{49}Ti^+$	0.1 ms	31.3–37.1 nm		193
Plant exposure											
2015	40 nm PVP-coated; 10, 12, 15, 20, 30, 40, 50, 80, and 100 nm citrate-coated Au NPs	Tomato plants	Enzymatic digestion with Macerozyme R-10, dilution	Meinhard nebulizer, cyclonic spray chamber	RF power 1600 W, cooling gas 18 L min^{-1}, auxiliary gas 1.2 L min^{-1}, nebulizer gas 1.08 L min^{-1}	Q	$^{197}Au^+$	0.1 ms	20 nm		194
2016	10 nm citrate-coated Ag NPs	*Arabidopsis thaliana* plants' roots and shoots	Enzymatic digestion with Macerozyme R-10, dilution	n/s	n/s	Q	$^{107}Ag^+$	0.05 ms	10 nm		195
2016	30–50 nm and 50–100 nm CeO_2 NPs	Shoots of cucumber (*C. sativus*), tomato (*S. lycopersicum* L.), soybean (*Glycine max*), pumpkin (*Cucurbita pepo*)	Enzymatic digestion with Macerozyme R-10	Meinhard nebulizer, cyclonic spray chamber	RF power 1600 W, cooling gas 18 L min^{-1}, auxiliary gas 1.2 L min^{-1}, nebulizer gas 1.06 L min^{-1}	Q	$^{140}Ce^+$	0.1 ms	23–25 nm		196

Table 1 (*Contd.*)

Year	NP types analyzed	Matrix	Sample preparation	Nebulizer and spray chamber	Plasma parameters	Mass analyzer	Measured isotopes	Dwell time	Size LOD (ESD)	Features	Ref.
2016	70 nm citrate-coated Pt NPs	*Lepidium sativum*, *Sinapis alba* plants	Enzymatic digestion with Macerozyme R-10, filtration (0.45 μm pore size), dilution	Meinhard glass microconcentric nebulizer, cyclonic spray chamber	RF power 1450 W, cooling gas 15.0 L min^{-1}, auxiliary gas 1.0 L min^{-1}, nebulizer gas 0.98 L min^{-1}	Q	$^{195}Pt^{+}$	0.1 ms	n/s		197
2017	Cu-containing NPs from fungicide residues (copper oxychloride)	Vine leaves	Rainfall washoff, through fall sampling, filtration (0.45 μm pore size), dilution	n/s	n/s	Q	$^{63}Cu^{+}$	0.1 ms	8–60 nm Cu		198
2017	17 nm PVP-coated Ag NPs	Soybean, rice (root and foliar exposures)	Enzymatic digestion with Macerozyme R-10, dilution	Meinhard nebulizer, cyclonic spray chamber	n/s	Q	$^{107}Ag^{+}$	0.05 ms	14 nm		199
2017	PVP-coated Ag_2S	Dicotyledonous cucumber (*Cucumis sativus*), monocotyladonous wheat (*Triticum aestivum* L.)	Enzymatic digestion with Macerozyme R-10, dilution	n/s	n/s	TQ	$^{107}Ag^{+}$	3 ms	20–25 nm		200
2018	20–100 nm CuO NPs	Leaves of vegetables, kale (*Brassica oleracea*, var. *Acephala Lacinato*), lettuce (*Lactuca sativa* var. green leaf cultivar), collard green (*Brassica oleracea*, var. *Acephala)*	Exposure to NPs, rinsing with ultrapure water or enzymatic digestion with Macerozyme R-10, dilution	Glass concentric nebulizer	RF power 1550 W, nebulizer gas 0.67 L min^{-1}, sampling position 8.0 mm	Q	$^{63}Cu^{+}$	0.1 ms	n/s		201
2018	Pd NPs	*Sinapis alba* leaves, stems, roots	Enzymatic digestion with Macerozyme R-10, filtration (0.45 μm pore size), dilution	Meinhard glass microconcentric nebulizer, cyclonic spray chamber	RF power 1450 W, cooling gas 15.0 L min^{-1}, auxiliary gas 0.9 L min^{-1}, nebulizer gas 1.10 L min^{-1}	Q	$^{105}Pd^{+}$	0.1 ms	25–30 nm		202

Table 1 (*Contd.*)

Year	NP types analyzed	Matrix	Sample preparation	Nebulizer and spray chamber	Plasma parameters	Mass analyzer	Measured isotopes	Dwell time	Size LOD (ESD)	Features	Ref.
2018	"Green synthesis" of Ag NPs	Leaf sap extract from *Aloe arborescens*	$AgNO_3$ addition to the leaf sap extract induces the formation of Ag NPs under sunlight, centrifugation, dilution	Concentric quartz nebulizer, baffle-type cyclonic spray chamber	RF power 1500 W, cooling gas 17 L min^{-1}, auxiliary gas 1.4 L min^{-1}, nebulizer gas 0.8 L min^{-1}	Q	$^{107}Ag^+$	5 ms	n/s		203
2018	Isotopically labelled Ag, Cu, ZnO NPs	*Arabidopsis thaliana* shoot and roots	Macerozyme R-10, filtration (0.22 μm pore size), dilution	MicroMist nebulizer	Cooling gas 15 L min^{-1}, auxiliary gas 1.0 L min^{-1}, nebulizer gas 1.05 L min^{-1}	Q	$^{107}Ag^+$, $^{65}Cu^+$, $^{70}Zn^+$	3 ms	n/s	Cu and ZnO NPs were not detected in shoots or roots because of the high background	204
2019	"Green synthesis" of Ag NPs	Cucumber leaf extract	$AgNO_3$ addition to the leaf extract, pH 10.0, 4 h at 80 °C	n/s	RF power 1550 W, nebulizer gas 0.67 L min^{-1}, sampling position 8.0 mm	Q	$^{107}Ag^+$	0.1 ms	n/s		205
2019	80–200 nm ZnO NPs	Lettuce *Lactuca sativa* L. growth medium, roots and leaves	Dilution, Macerozyme R-10 for roots and leaves	n/s	n/s	Q	$^{66}Zn^+$	0.1 ms	n/s		206
Model soil samples											
2014	25 nm PVA-coated Ag NPs, 30 nm ZnO NPs, 42 nm TiO_2 NPs, 35 nm CeO_2 NPs	Soil spiked with biosolids that were enriched with NPs	Spiking, water extraction, centrifugation, filtration (0.45 μm pore size)	n/s	n/s	Q	n/s	10 ms	18 nm Ag, 70–80 nm TiO_2, 10 nm CeO_2		207
2015	CuO NPs	Spiked topsoil colloid extracts	Extraction, dilution, spiking	MicroMist nebulizer	RF power 1550 W, cooling gas 15 L min^{-1}, auxiliary gas 0.15 L min^{-1}, nebulizer gas 0.98 L min^{-1}	Q with KED (He)	$^{63}Cu^+$	5 ms or 0.1 ms	15 ± 10 nm		208
2017	10, 30, 60 nm citrate-coated Au NPs, 30 nm BPEI- and PVP-coated Au NPs	Spiked soil colloidal extracts	Water extraction, centrifugation, filtration (0.45 μm pore size), spiking, CPE	Concentric MicroMist nebulizer, Scott spray chamber	n/s	Q	$^{197}Au^+$	10 ms	n/s		209
2017	40 nm PVP-coated Ag NPs	Natural sandy loam soil spiked with biosolids that were enriched with NPs	Spiking, TSPP extraction, gravimetric sedimentation, dilution	Low pressure PFA nebulizer	RF power 1600 W, nebulizer gas 1.04 L min^{-1}	Q	$^{107}Ag^+$	0.05 ms	20 nm		210

Table 1 (*Contd.*)

Year	NP types analyzed	Matrix	Sample preparation	Nebulizer and spray chamber	Plasma parameters	Mass analyzer	Measured isotopes	Dwell time	Size LOD (ESD)	Features	Ref.
2017	40 nm PVP-coated Ag NPs	Nanopure water with $NaNO_3$ and KNO_3, filtered sandy loam soil extracts with $NaNO_3$ and KNO_3	KNO_3 extraction, centrifugation, filtration (0.45 μm and 0.22 μm pore size), spiking, dilution	Low pressure PFA nebulizer, cyclonic spray chamber	RF power 1600 W, nebulizer gas 1.04 L min^{-1}	Q	$^{107}Ag^+$	0.05 ms	19 nm		211
2017	25 and 40 nm PVP-coated Ag NPs	Spiked sandy loam soil and biosolid extracts	Spiking, TSPP extraction, sonication, filtration (0.45 μm and 0.22 μm pore size), dilution	Low pressure PFA nebulizer, cyclonic spray chamber	RF power 1600 W, nebulizer gas 1.04 L min^{-1}	Q	$^{107}Ag^+$	0.05 ms	19 nm	Optimization of the NP extraction conditions from soil, only the most efficient conditions were mentioned	212
2018	30 nm citrate-, BPEI-, PVP-, PEG-, NOM-coated Au NPs	Standard soil water extracts, estuarine sediment in moderately hard water	Spiking, moderately hard water extraction, centrifugation, dilution	Concentric nebulizer, Scott spray chamber	n/s	Q	$^{197}Au^+$	10 ms	n/s		213
2018	40 and 100 nm citrate-coated; 75 and 100 nm PVP- and PEG-coated Ag NPs	Consumer product (band aid) water extracts, spiked soil water extracts	Spiking, Milli-Q water extraction, filtration (0.45 μm pore size)	n/s	RF power 1500 W, cooling gas 15 L min^{-1}	Q	$^{107}Ag^+$	10 ms	n/s		214
Solid environmental samples											
2016	As-containing NPs	Leachate from mine wastes	Leaching with 1 mM KCl, centrifugation	Glass concentric slurry nebulizer, cyclonic spray chamber	RF power 1200 W, cooling gas 15 L min^{-1}, auxiliary gas 1.2 L min^{-1}, nebulizer gas 1.0 L min^{-1}	Q	$^{75}As^+$	5 ms	117 nm $Fe^{III}As^{V}O_4 \cdot 2H_2O$	Settling time of 3 ms	215
2017	Zn-, Fe-, and Ti-containing NPs	Sewage sludge	Acetic acid extraction, dilution	n/s	n/s	Q with KED for $^{56}Fe^+$	$^{47}Ti^+$, $^{66}Zn^+$, $^{56}Fe^+$	0.1 ms	15–20 nm Ti, 15–16 nm Zn, 12–17 nm Fe		216
2017	Ce-containing natural NPs and <50 nm CeO_2 NPs	Spiked topsoil samples	Spiking, shaking, wet-sieving (32 μm pore size), freeze-drying, aqueous colloid extraction, dilution	Pneumatic nebulizer, cyclonic spray chamber for TOF, Miramist nebulizer for Q	RF power 1400 W, cooling gas 16 L min^{-1}, auxiliary gas 1.1 L min^{-1}, and nebulizer gas 1.2 L min^{-1} for TOF; RF power 1550 W, cooling gas 15 L min^{-1}, auxiliary gas 0.4 L min^{-1}, and	TOF at 33 kHz complete mass spectrum in 300 μs, Q	MA for TOF; $^{140}Ce^+$ and $^{139}La^+$ for Q	n/a for TOF, 5 ms for Q	0.10–0.17 fg Ce, 0.13 fg La for TOF; 0.13–0.57 fg Ce, 0.21–0.34 fg La for Q	Natural and engineered NPs were identified with multielement fingerprinting	72

Table 1 (*Contd.*)

Year	NP types analyzed	Matrix	Sample preparation	Nebulizer and spray chamber	Plasma parameters	Mass analyzer	Measured isotopes	Dwell time	Size LOD (ESD)	Features	Ref.
					nebulizer gas 0.8 L min^{-1} for Q						
2018	Pt NPs	Road dust leachate, catalyst material	Ultrasonic extraction with stormwater runoff, filtration (0.45 μm pore size)	Quartz nebulizer	n/s	Q	$^{195}Pt^{+}$	5 ms	7.4 nm		217
2019	Th- and U-containing NPs	Leachates of tailings of a niobium mine	Leaching with different solutions of 2–10 pH; Ca, Mg, and Na at 0–13 mmol L^{-1}; fulvic acid at 0–20 ng L^{-1}; centrifugation	n/s	RF power 1300 W, cooling gas 13 L min^{-1}, auxiliary gas 1.2 L min^{-1}, nebulizer gas 0.7–1.0 L min^{-1}	SF	$^{232}Th^{+}$, $^{238}U^{+}$	0.05 ms	3 nm U, Th		218
Model water samples											
2013	1–10 nm sodium polyacrylate-coated; 20, 40, and 80 Ag NPs	NP water suspensions	Dilution	n/s	n/s	Q	n/s	3 ms	20 nm		219
2015	100 nm citrate-coated Ag NPs; 60, 100 nm Au NPs, Au/Ag 48 nm core/ 15 nm shell	Spiked water with laundry detergents	Spiking, filtration or no filtration, dilution	Type-C MiraMist nebulizer, cyclonic spray chamber	n/s	Q	n/s	3 ms	30 nm Ag		220
2015	252 nm DNA/ SiO_2 NPs, 350 nm SiO_2 NPs	Spiked ultrapure and drinking water	Dilution	Quartz MicroMist nebulizer, cyclonic spray chamber	RF power 950 W, cooling gas 16 L min^{-1}, auxiliary gas 0.6 L min^{-1}, nebulizer gas 1.2 L min^{-1}	SF	$^{28}Si^{+}$	5 ms	n/s		221
2017	60, 100 nm citrate- and PVP-coated Ag NPs and their aggregates	$NaNO_3$ or $NaNO_3$ and $Ca(NO_3)_2$	Dilution or dialysis	MicroMist nebulizer	RF power 1400 W, cooling gas 18.0 L min^{-1}, auxiliary gas 1.30 L min^{-1}, nebulizer gas 1.44 L min^{-1}	Q	n/s	10 ms	n/s		222
Other applications											
2016	Cu_2O NPs	Antifouling paint	Dilution, sonication	n/s	n/s	Q	n/s	0.1 ms	n/s		223
2016	Ag NPs	Release from plastic food containers into	Incubation	n/s	Sampling position 7 mm	n/s	n/s	3 ms	n/s		224

Table 1 (*Contd.*)

Year	NP types analyzed	Matrix	Sample preparation	Nebulizer and spray chamber	Plasma parameters	Mass analyzer	Measured isotopes	Dwell time	Size LOD (ESD)	Features	Ref.
		food simulants (Milli-Q water, 10% ethanol, 3% acetic acid)									
2016	Ag NPs	Release from plastic food containers and baby feeding bottles into food simulants (Milli-Q water, 10% and 90% ethanol, 3% acetic acid)	Incubation, sonication, evaporation of ethanol and reconstitution in Milli-Q water	MicroMist nebulizer, Scott spray chamber	RF power 1550 W, cooling gas 15 L min^{-1}, auxiliary gas 1.2 L min^{-1}, nebulizer gas 1 L min^{-1}	Q	$^{107}Ag^{+}$	10 ms	n/s		225
2016	Ag NPs	Release from nanosilver conductive ink, ink itself	Ink dilution	n/s	n/s	Q	n/s	0.1 ms	n/s		226
2017	Ag NPs	Glass slides coated with Ag NPs, structured SiO_2-based nanocomposites with a single layer of Ag NPs	Ultrapure water extraction and dilution for glass slides; MOPS extraction, algae treatment, centrifugation, dilution for nanocomposites	Glass concentric slurry nebulizer, cyclonic spray chamber	RF power 1200 W, cooling gas 15 L min^{-1}, auxiliary gas 1.2 L min^{-1}, nebulizer gas 1.0 L min^{-1}	Q	$^{107}Ag^{+}$ and $^{109}Ag^{+}$	5 ms	24 to 40 nm		227
2017	Ag NPs	Toothbrushes	Release of NPs to tap water	n/s	Sampling position 7 mm	n/s	n/s	3 ms	35 nm		228
2017	TiO_2 NPs	Textiles (table placemats, wet wipes, microfiber cloths, and baby bodysuits)	Release of NPs into deionized water, sonication, shaking, dilution and addition of Triton-X	n/s	n/s	n/s	$^{48}Ti^{+}$, $^{44}Ca^{+}$	0.1 ms	27–33 nm		229
2017	Iron based Fe_2O_3 nanopigment	Nanopigments in a polymer matrix: release from cryo-milled debris into Milli-Q water, moderately hard water, water with a humic acid	Rotation end over end	MicroMist nebulizer	RF power 1550 W, cooling gas 15 L min^{-1}, auxiliary gas 0.19 L min^{-1}, nebulizer gas 0.98 L min^{-1}	Q with KED (H_2)	$^{56}Fe^{+}$	5 ms	n/s		230
2017	Ag NPs	Release from antibacterial leather	Milli-Q water extraction	n/s	n/s	Q	$^{107}Ag^{+}$	0.05 ms	n/s		231

Table 1 (*Contd.*)

Year	NP types analyzed	Matrix	Sample preparation	Nebulizer and spray chamber	Plasma parameters	Mass analyzer	Measured isotopes	Dwell time	Size LOD (ESD)	Features	Ref.
		and leatherette into Milli-Q water									
2017	TiO_2, Al_2O_3, Cu-phthalocyanine, and CuO NPs	Tattoo inks	Dilution	PFA-ST nebulizer	RF power 1400 W, cooling gas 15 L min^{-1}, auxiliary gas 1.2 L min^{-1}, nebulizer gas 1.05 L min^{-1}	Q with KED (He)	$^{27}Al^+$, $^{63}Cu^+$, $^{47}Ti^+$	5 ms	n/s		232
2017	Mo- and Fe-containing NPs	Asphaltene solutions	Dilution with *o*-xylene, sonication	Concentric glass nebulizer	RF power 1600 W, nebulizer gas 0.35 L min^{-1}, option gas 0.35 L min^{-1} (Ar, 80%; O_2, 20%), sampling position 10 mm	TQ	$^{51}V^+$, $^{56}Fe^+$, $^{60}Ni^+$, $^{95}Mo^+$	0.1 ms	n/s		233
2017	Pt/SiO_2 nanocomposite with ultra-small Pt NPs	Pt/SiO_2 nanocomposite	Dilution	MicroMist pneumatic nebulizer, Scott-type spray chamber	RF power 1500 W, nebulizer gas 1.05 L min^{-1}, sampling position 8.0 mm	Q with KED (He)	$^{195}Pt^+$	10 ms	17.2 nm Pt		234
2018	Al-, Si-, and Ti-containing NPs	Release from ceramic cookware during simulated linear abrasion	Wash with Liquinox, release into 3% acetic acid, dilution	MicroMist nebulizer	n/s	TQ	$^{27}Al^+$, $^{28}Si^+$, $^{48}Ti^+$	3 ms	n/s	H_2 was used as a reaction gas	235
2018	Ag NPs	Consumer sprays	Dilution	n/s	n/s	Q	n/s	10 ms	17.3–35.3 nm		236
2018	Sb-, Pb-, and Ba-containing NPs	Gunshot residue wash from shooters' hands	Wash with ultrapure water with 0.2% formaldehyde or hand swabbing with cotton swabs and sonication	n/s	n/s	Q	$^{121}Sb^+$, $^{137}Ba^+$, $^{208}Pb^+$, $^{121}Sb^+$ and $^{137}Ba^+$, $^{121}Sb^+$ and $^{208}Pb^+$, $^{137}Ba^+$ and $^{208}Pb^+$, $^{206}Pb^+$ and $^{208}Pb^+$, $^{207}Pb^+$ and $^{208}Pb^+$, $^{206}Pb^+$ and $^{207}Pb^+$	29 μs (Sb, Ba), 30 μs (Pb)	n/s	Single and dual element modes were used. Monitoring of two isotopes with 145 μs settling time, 150 μs settling time for lead isotopes	237
2018	As-containing NPs	Cigarette smoke	Smoke collection with electrostatic trapping, wash with methanol, dilution with deionized water	Dual-port spray chamber	n/s	Q	$^{75}As^+$	0.1 ms	n/s	No As-containing NPs were found	238

Table 1 (*Contd.*)

Year	NP types analyzed	Matrix	Sample preparation	Nebulizer and spray chamber	Plasma parameters	Mass analyzer	Measured isotopes	Dwell time	Size LOD (ESD)	Features	Ref.
2018	Biogenic Se NPs; 50 and 100 nm Se NPs	Se-rich yeast	Enzymatic digestion with Driselase, protease	Concentric nebulizer, cyclonic spray chamber	RF power 1550 W, cooling gas 15 L min^{-1}, auxiliary gas 0.9 L min^{-1}, nebulizer gas 1.10 L min^{-1}	Q with KED (H_2)	$^{78}Se^+$, $^{80}Se^+$	5 ms, 0.1 ms	18 nm		239
2018	Cu NPs	*Cuprum metallicum*, *Gelsemium sempervirens* homeopathy medicines	n/s	n/s	n/s	Q	n/s	n/s	45 nm Cu, 52 nm Cu_2O		240
2019	Niobium and titanium carbonitride particles	Microalloyed steel	Etching in H_2SO_4 and Disperbyk-2012, centrifugation to remove dissolved iron, dilution	Pneumatic nebulizer, cyclonic spray chamber	n/s	TOF at 555 Hz	Ma, $^{48}Ti^+$, $^{93}Nb^+$	n/a	27.5 nm NbCN, 50.5 nm TiNbCN		241

[a] Note that the entries are grouped by the sample matrix that is the main focus of each study. Papers that report solely on spICP-MS method development are not included.

2.2 Sample introduction

In an ideal world, a sample introduction system would exist for spICP-MS that features a 100% transport efficiency and a high tolerance to all kinds of different matrices. Today, commercially available nebulizers do not achieve a 100% particle transport efficiency, which necessitates the precise determination of the nebulizer transport efficiency for system calibration. Pneumatic nebulizers achieve only approximately 0.5–2% transport efficiency with a 1 mL min^{-1} sample uptake rate.[27] The aerosol transport through a spray chamber is aimed to eliminate larger droplets, which helps to reduce the solvent load and to improve analyte signal stability, but at the same time a considerable amount of the analytes is also lost. An alternative to high-flow pneumatic nebulizers (*e.g.* 1 mL min^{-1} sample uptake rate) are micronebulizers with considerably lower sample flow rates. With micronebulizers (*e.g.* at a 10 μL min^{-1} sample uptake rate) the transport efficiency can be improved to 60 or up to 80%.[27] Micronebulizers utilize low-volume spray chambers (*e.g.* 15 cm^3) and help to improve the transport efficiency. For example, a transport efficiency of approximately 93% was reportedly achieved for 70 nm Pt NPs with a large-bore concentric nebulizer and a small-volume on-axis cylinder chamber.[28] A loss of 7% was discussed to be likely due to adsorption to nebulizer and spray chamber walls, NP surface charges, and assumptions made during PNC determination.[28] In general, the higher the sample flow of a nebulizer, the lower its transport efficiency typically is. However, the matrix tolerance decreases from higher to lower sample uptake rates. Micronebulizers can be more difficult to operate and maintain due to the dimensions of the inlet capillary (*e.g.* 0.15 mm),[28] which might get obstructed, and sample interchange can also be tedious. When compared to standard pneumatic nebulizers, however, micronebulizers are considered to be advantageous in the field of spICP-MS for low-volume samples and simple matrices, when they are used to interface with separation devices, or to achieve lower PNC LODs.

Another approach to achieve high transport efficiency for NPs is through a microdroplet generator (MDG), in which monodisperse droplets are generated by a piezoelectrically actuated quartz capillary.[29] The droplets generated at a controlled volume and speed are transported into the ICP, and a transport efficiency of over 95% can be achieved.[30] The advantage of the MDG introduction is that calibration may be performed with dissolved metal standards if reference materials of the NPs are not available.[30,31] Also, a combination of a pneumatic nebulizer and an MDG was recently reported as a means to exchange different sample matrixes faster and to calibrate the NP signal using traceable elemental standards without the need to use NP reference materials.[31,32] In this setup, the MDG was used for system calibration, and the pneumatic nebulizer was used for sample introduction.

A comparison of pneumatic nebulizers and MDG-based sample introduction systems was performed in order to highlight the advantages and disadvantages of the techniques for NP quantification.[33,34] It was found that losses are still possible at the sample introduction stage affecting both NPs and dissolved

species. Future improvements of sample introduction systems are still needed to ensure high NP and dissolved ion transport efficiency, robust operation, automated sample introduction, and a high tolerance toward different matrices.

One approach to the introduction of solid samples into the ICP-MS is laser ablation (LA). Recent research has demonstrated a possible coupling of LA to spICP-MS.[35] Instrumental parameters were optimized, and imaging of a sunflower plant root (cross section), which was previously exposed to Au NPs (60 nm citrate-coated, PNC: 1.83×10^9 NP mL^{-1}), has been performed. With 307 000 data points obtained per line scan, the obtained results show that Au NPs retained their original size and were concentrated on the surface of the root and rhizodermis (Fig. 2). It is recommended by the authors of the study "that the laser fluence is kept below 1 J cm^{-2} to avoid NP degradation".[35]

2.3 NPs in the ICP source

When NPs enter the ICP, they would ideally get fully vaporized, atomized, and ionized, regardless of their elemental composition, size, and matrix they are in. However, it is important to consider differences in the physicochemical properties of the elements (and other species such as their oxides) that the particles are made of including boiling points and ionization potentials. These differences are likely to result in different optimal experimental conditions for the best spICP-MS performance. In fact, the fundamental aspects of micrometer-sized particles were studied by LA-ICP-MS and it was found that the particle size can significantly affect the vaporization, atomization, and ionization efficiency.[36,37] While our understanding of the behavior of micrometer-sized particles in the ICP has improved in recent years, the number of fundamental studies on the effects of nanometer-sized particles in spICP-MS is still very limited. For example, Ho *et al.* focused on the determination of the maximum signal intensity as a function of the ion sampling position (frequently referred to as "sampling depth") for different elements in aqueous solution and a selection of Au and ZrO_2 NPs.[38] It was shown that different elements have a different signal maximum in their sampling position profiles depending on the combination of element ionization potentials and boiling points of the corresponding oxides. 150 nm and 250 nm Au and 80 nm ZrO_2 NPs were investigated in the same study, and they were found to have different complete ionization positions (±0.5 mm) in the ICP compared to dissolved metal analysis (Fig. 3).[38] Consequently, when calibration with dissolved metals is performed in spICP-MS, it is important to determine the position of the maximum signal in sampling position profiles for method optimization and minimization of systematic errors.

Incomplete ionization may occur due to a relatively larger mass of individual NPs, and, in turn, would lead to a limited upper size dynamic range for NP analysis. Additionally, matrix ions that reach the plasma together with the NPs may affect the ionization of the NPs. For example, Niemax *et al.* utilized an

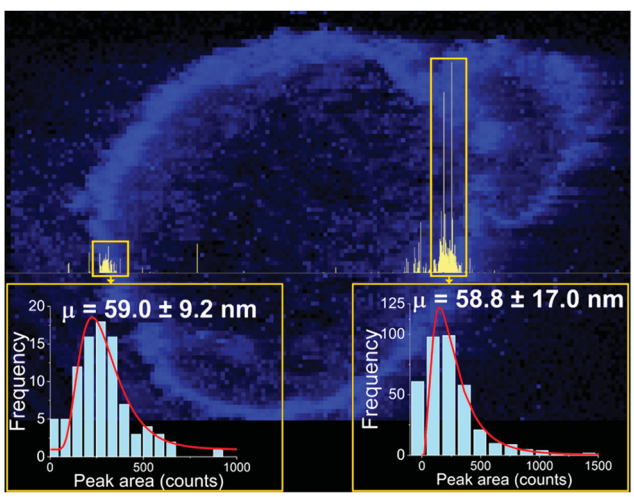

Fig. 2 Image (in blue) showing the distribution of gold in a root cross section from a sunflower plant exposed to gold NPs with a mean size of 60 nm, overlaid with a high-resolution time-resolved signal of a single LA-spICP-MS line scan (in yellow). The pixel size in the image is 5×5 μm^2, and the line-scan signal was recorded every 100 μs. Reprinted with permission from Metarapi *et al.*[35] Copyright 2019 American Chemical Society. (https://pubs.acs.org/doi/10.1021/acs.analchem.9b00853, further permissions related to the material excerpted should be directed to the American Chemical Society).

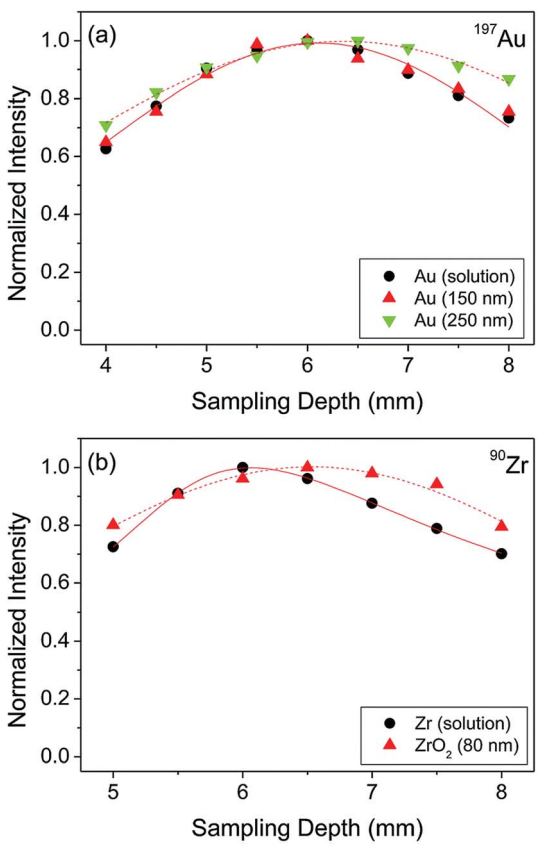

Fig. 3 Sampling depth profiles of (a) Au and (b) Zr in the form of aqueous solution with a concentration of 10 μg L^{-1} and discrete NPs. Reproduced from Ho *et al.*[38] with permission from the Royal Society of Chemistry.

MDG to study atomization processes in the plasma.[39] They reported a local plasma cooling effect during atomization which is dependent on the analyte mass. Another finding was that the matrix elements in the droplets affect the droplet atomization. Later they confirmed experimentally that the position of atomization and ionization of analytes in the ICP strongly depends on the injector gas flow, the size of the introduced droplet, and also on the mass of the analyte (*e.g.* particles).[40] The presence of a matrix (SiO_2 particles in a Ca^{2+} matrix) affects both particle and matrix component atomization. For example, there was a delay in complete atomization of two 1.55 μm SiO_2 particles compared to one 0.83 μm SiO_2 particle that translates into "a spatial shift of about 8 mm in the ICP."[40] It has also been shown that the position of atomization and ionization is important for ion sampling. If the ions are sampled too early, when atomization and ionization are still not complete, then the detected signal per particle decreases. If the sampling is performed too late, then after the particles are ionized, diffusion occurs, and the signal per particle may also decrease.[27]

Ho *et al.* performed a simulation study focusing on incomplete particle vaporization.[41] It was shown that ion sampling requires knowledge of the point of complete particle ionization. For example, they reported that the mass calibration leveled off at higher mass values (above 34 fg) at the 8 mm sampling position and concluded that Au particles larger than 150 nm may experience incomplete ionization; further experiments to confirm this hypothesis were not conducted in the study. A sampling position upstream in the plasma (closer to the coil) resulted in an even narrower linear dynamic range (LDR) for Au NP detection (*e.g.* 6 mm in the simulations results in incomplete vaporization of Au NPs above 60 nm). Additionally, smaller NPs are subjected to diffusion to a greater extent, causing analyte losses for smaller particles that already completely vaporize early in the ICP. Therefore, it was pointed out that it is important to match the NP masses used for calibration with the analyzed particles. A literature search[41] was done to determine the detected signal of the particles at which the size calibration is no longer linear (100 nm for Ag NPs[34] and 150 nm for Au NPs[41]); however, to what extent incomplete particle ionization and the limited LDR of the detector influence the obtained values was not studied. Borovinskaya *et al.* demonstrated that droplets that are off the central axis of the plasma experience a temporal shift in their ICP-MS signals due to diffusion in the plasma.[42] A computational study confirmed the advantages of introducing the samples on-axis to achieve higher transport efficiencies of the ions into the MS.[43] Chan and Hieftje demonstrated that injection of droplets (deionized water) into the ICP causes a noticeable influence on it; the plasma is locally cooled (the cooling lasts for more than 2 ms after the droplet leaves the load-coil) and is then reheated to a temperature above equilibrium (this effect lasts up to 4 ms after the droplet leaves the load coil); therefore, these effects last longer than the residence time of droplets in the plasma.[44] Here, the OH molecular band and Ar I and H I emission lines were measured with a monochromatic imaging spectrometer every 100 μs.

The studies presented in the paragraph above demonstrate that it is indeed important to optimize the plasma conditions for a precise and sensitive NP detection. For example, the injector gas flow (only Ar and not He was considered in this review), plasma power, sampling position, and injector diameter should be optimized based on the analytes and matrix used. Other studies were done to find an optimal sampling position. They studied the effect of the ICP-MS sampling position on the signal intensity of Ag and Au NPs.[45] It was shown that it is necessary to optimize the sampling position because it can decrease the size LODs by 25–30% for the studied NPs compared to the standard instrument tuning procedure. For example a sampling position of 4 mm was found to be optimal for Ag and Au NPs to obtain the highest signal intensity, and the signal of dissolved silver and gold standards followed the same trend.[45] It is important to note that the optimal sampling position would be different for different instruments, and the elements of different mass ranges, and the formation rate of doubly charged ions and oxides should be accounted for some elements. Chun *et al.* used a double-viewing-position single particle ICP-OES approach to study and select an appropriate sampling position.[46] The approach can be used to elucidate a potentially incomplete ionization of particles, and, therefore, provides information for spICP-MS that sampling from these positions would not be suitable.

spICP-MS is highly dependent on the plasma conditions, and more studies are required in this respect to develop robust protocols to establish optimal plasma conditions for different NPs and different matrices. The plasma conditions that were used in spICP-MS application papers are summarized in Table 1 and discussed in the corresponding chapter. Apart from the choice of the nebulizer, torch injectors of a smaller diameter (1 or 1.5 mm inner diameter) may help to guide NPs on a central axis movement towards the sampler tip. The combination of three parameters, namely injector gas flow, plasma power, and ion sampling efficiency (depending on sampling position), significantly affects NP ionization and, in turn, the recorded signals, and should be optimized prior to analyses. The aim is to achieve the conditions under which the ionization is complete for the required NP size range in a specific matrix, and to sample the ions into the MS from the point of complete ionization to limit ion cloud diffusion in the plasma and a loss of ions per particle.

2.4 Ion transport

All analyte ions produced in the ICP would ideally be transferred completely into the mass spectrometer. However, the step of ion extraction is associated with losses. Ion extraction from the atmospheric-pressure ICP is typically performed by using a two-stage (sampler and skimmer cones) and sometimes a three-stage aperture interface. Downstream of the skimmer orifice, positively charged analyte ions are separated from other plasma species using ion guide devices. While optimal ion lens voltages may differ from element to element, typically a standard tuning protocol is established with a multielement solution to determine only one "ideal" set of voltages for the whole mass range. The maximum sensitivity for a particular ion may be achieved by fine tuning. Additionally, space charge effects,

namely ion losses due to charge repulsion and defocusing of the ion beam downstream of the skimmer and the ion optics, may introduce mass-dependent artifacts in nanoparticle analysis similarly to what is known for standard elemental analysis. Niu and Houk[47] described fundamental aspects of ion extraction in ICP-MS, and highlighted that the understanding of the processes occurring during the transport of the ions to the mass analyzer would help to reduce ion losses at this stage. Typically, low-mass isotopes have lower ion kinetic energies compared to high-mass isotopes; therefore, low-mass isotopes get forced out to the edges of the ion beam by high-mass isotopes and a relative loss of sensitivity for low-mass isotopes is observed.[48] To the best of our knowledge, papers on space-charge effect investigations specifically for NP analysis have not been published yet. Clearly, such ion sampling and transport effects as are mentioned above will affect ions from NPs in a similar fashion, and, in turn, lead to possible partial losses of the number of ions per NP that were generated in the plasma, partial losses of the background ions, losses due to the extraction of positively charged ions, space charge effects *etc.* All of these losses will likely decrease the overall instrument sensitivity and contribute to an increase in the size LOD for NPs in spICP-MS. However, the order-of-magnitude compared to other fundamental aspects in spICP-MS is not clear to date and more fundamental research is required.

2.5 Mass analyzers

An ideal mass analyzer for NPs would be able to have a high mass resolution to provide isotopic information along with simultaneous rapid multielement detection of short (few hundreds of microseconds)[10] NP signals. The mass analyzers that are available today are suitable for different types of applications and still have some room for improvement. ICP-Q-MS is widely used because of its comparatively low cost and capability for fast NP detection. However, ICP-Q-MS instruments are limited in terms of multielement detection and resolution (one m/z unit at a time). Switching between different m/z ratios requires some settling time (on the order of 100 μs)[49] for the new set of conditions to be stable (ion travel time through the mass analyzer *etc.*). If one decides to perform isotope-hopping over the course of a fast transient NP signal, the settling time leads to a limited signal coverage, which also significantly limits the number of counts detected per NP. A proof-of-concept for a two-element detection was recently demonstrated, where Au/Ag core/shell NPs were detected with 100 μs dwell time and 100 μs settling time.[49] Interference is another limitation of ICP-Q-MS due to its comparatively low mass resolution. A large number of elements suffer from interference in ICP-Q-MS,[50] especially in the presence of a matrix. If the interfering species is present only as the background and not in the form of NPs, then NPs could still be detected to a certain extent as signal pulses above the continuous background. However, as the variation of the background signal rises with increasing signal level,[51,52] the NP size LOD rapidly increases (from 18 nm to 32 nm for Ag NPs, when 0.3 μg L^{-1} Ag^+ was added, and 5 ms dwell time).[53] One approach to remove interference may be the use of a collision-reaction cell with kinetic energy discrimination. The collision-reaction cell was purposely used to reduce the sensitivity of the instrument to be able to detect Au NPs up to 200–250 nm in diameter.[54,55] After passing through the mass analyzer, the ion detection itself is performed usually by using a discrete dynode electron multiplier. The crucial parameter to set here is the detector dwell time, which will be discussed in the next chapter. In spite of all limitations discussed above, ICP-Q-MS is still the most widely used instrument (compared to other mass analyzers) for NP detection in terms of the number of publications.

The utilization of triple quadrupole (TQ or QQQ) technology allows overcoming matrix interference not only in solution analysis but also in particle analysis. For example, the use of CH_3F or H_2 for reactions/collisions in ICP-QQQ-MS allowed quantifying SiO_2 NPs (high natural background of N_2) in the range from 80 to 400 nm using on-mass detection with H_2 ($^{28}Si^+$) and mass-shift detection with CH_3F ($^{28}Si^{19}F^+$) and significantly improved the size LODs (Fig. 4).[56] TiO_2 NPs can be quantified with the use of NH_3 as the reaction gas in candy products[57] and water matrices with a high Ca content[58] ($^{48}Ca^+$ interferes with the most abundant $^{48}Ti^+$ isotope, and the mass-shift detection of $[^{48}Ti(^{14}N^1H_3)_3(^{14}N^1H)]^+$ has been performed). In contrast to ICP-Q-MS and ICP-QQQ-MS, sector field (SF)-ICP-MS and multicollector instruments feature a higher mass resolution and sensitivity compared to ICP-Q/QQQ-MS and can also be used for NP detection.[30,58–64] For example, a high mass resolution makes it possible to distinguish $^{48}Ti^+$ ($m/z = 47.948$) and $^{48}Ca^+$ ($m/z = 47.953$) during the analysis of TiO_2 NPs in calcium rich matrices.[58] The feasibility of spICP-MS for isotope analysis in erbium oxide particles was demonstrated with multi-collector (MC)-ICP-MS.[65] Isotope dilution analysis was introduced for Ag NP analysis and quantification with ICP-Q-MS.[66,67] Here, spiked samples with isotopically enriched $^{109}Ag^+$ solution were introduced for quantification.

A limitation of scanning-type mass analyzers is the fact that only one isotope (m/z) can be examined at once. Quasi-simultaneous multielement analysis can be performed with time-of-flight ICP-MS (ICP-TOF-MS).[68] While ICP-TOF-MS instruments were offered by manufactures in the past but did not seem to find their way into the routine elemental analysis market, the recent interest in nanoparticle analysis led researchers to revisit this type of mass analyzer. A prototype instrument was developed by the Günther group at ETH Zurich which features a 30 kHz spectral acquisition rate. Particle size LODs of 46 nm, 32 nm, and 22 nm for Ag, Au, and U NPs respectively were reported (at that time higher than that with ICP-Q-MS[34,69,70]). In a follow-up study, ICP-TOF-MS was used to perform the analysis of *e.g.* Au/Ag core/shell NPs. It was successfully shown that this core/shell material could be identified even in the presence of Ag NPs in the same sample. Improved size-related LODs of 19 nm and 27 nm for Au and Ag NPs respectively were reported (values determined with Poisson statistics).[71] The benefit of all-isotope-information in a sampled ion cloud was recently exploited to distinguish natural from engineered CeO_2 NPs[72] (Fig. 5) and TiO_2 NPs.[73] The commercial ICP-TOF-MS is reported to achieve 29 nm, 14 nm, and 7 nm

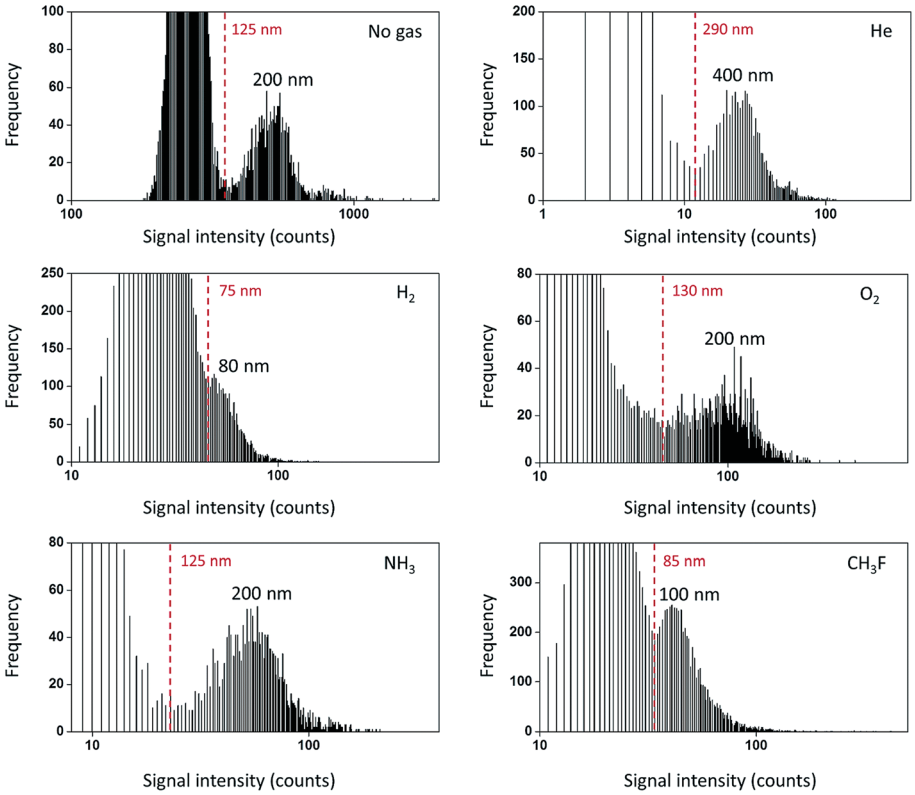

Fig. 4 Frequency distribution for the lowest NP sizes detectable using different reaction gases in ICP-TQ-MS for SiO_2 particle analysis. Practical $LODs_{size}$ are indicated in red in each figure. Frequency refers to the number of events of each type (background or NPs) detected. Reproduced from Bolea-Fernandez *et al.*[56] with permission from the Royal Society of Chemistry.

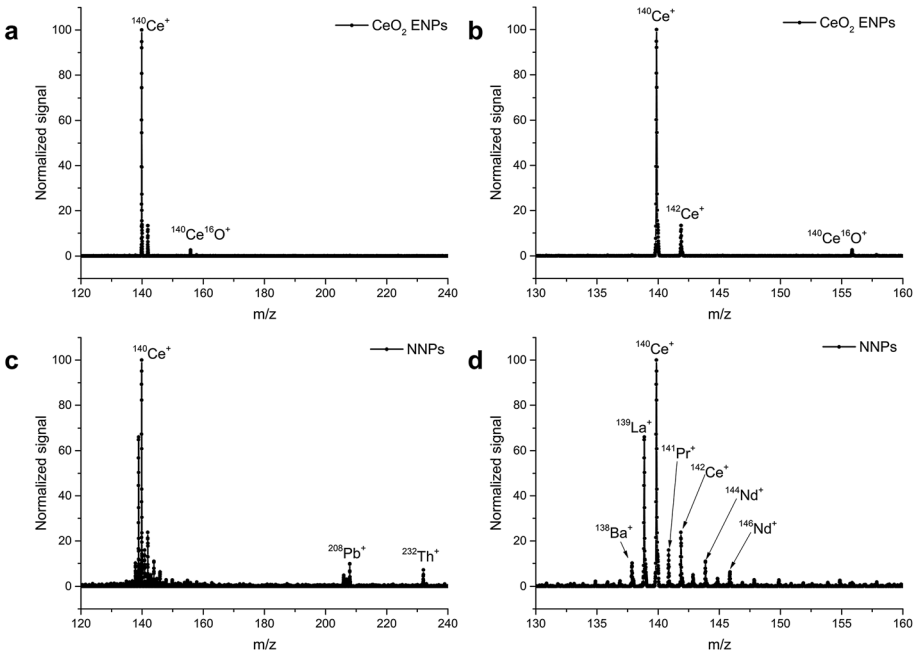

Fig. 5 ICP-TOF-MS mass spectra of CeO_2 engineered NPs and natural Ce-containing NPs. Averaged mass spectra for 20 discrete single nanoparticle events from both a suspension of CeO_2 engineered NPs (a and b (zoomed on Ce)) and a pristine soil sample with natural Ce-containing NPs (c and d (zoomed on Ce and neighboring isotopes)). The engineered NP sample is characterized solely by the Ce ion signal, while the geogenic Ce-containing NNP sample shows, in addition to the Ce signal, detectable levels of La, Ba, Pr, Nd, and Th within single-particle events. Reproduced from Praetorius *et al.*[72] with permission from the Royal Society of Chemistry.

LODs for Ti, Mo, and Au containing NPs respectively.[74] It was used, for example, for Bi containing NPs and NPs of steel to obtain the elemental composition of these industrial materials.[74]

2.6 Detector dwell time

Ideally, spICP-MS requires fast time-resolved detection to get accurate information (number of counts) for each detected NP over the whole required duration of the measurement. In this paper, we focus on secondary electron multiplier (SEM) detectors as they are most frequently used for ICP-Q-MS. Usually, ion detection occurs sequentially within defined time intervals called dwell times. In spICP-MS, dwell times in the millisecond time range are still the most frequently used (Table 1, also determined by the available settings of the instruments). As was demonstrated earlier, for example in a study on the effect of a CE buffer matrix on the particle ion cloud duration in CE-spICP-MS,[10] NPs typically result in ion cloud event durations on the order of a few hundreds of microseconds. One fundamental limitation of millisecond dwell times is that only one data point is used to describe a shorter transient. Additionally, a dead time between the individual dwell times[5] may interrupt the time-resolved measurements and lead to count losses in pulse-counting mode of the SEM. The occurrence of a NP between two adjacent dwell time intervals may cause one NP to be detected as two smaller ones (split-particle events). Similarly, towards higher particle numbers in a suspension, two or more particles may fall into one dwell time (particle coincidence), which results in a skewed PNC. Therefore, the users of millisecond dwell times in spICP-MS should always consider a suitable PNC range for their measurements and be aware of the limitations of the method when the data are used to draw conclusions *e.g.* from particle stability and toxicology studies.

One possible approach to overcome the measurement artifacts is to use integration times that are significantly shorter than the duration of NP ion clouds (on the microsecond time scale). This way allows for obtaining time-resolved profiles of NP ion clouds with an adequate number of data points per transient. The main challenge then arises in the data acquisition, storage, and processing of μs time-resolved data. For example, if the dwell time would be 10 μs, then each 1 s 100 000 data points are obtained. Therefore, a special data processing for visualization and quantification is required that is different from standard ICP-MS data acquisition (DAQ) and software, respectively. In addition, the accurate extraction of NP ion clouds and their unambiguous identification above possible background counts are critical in μs-spICP-MS. To the best of our knowledge, the first system for time-resolved particle analysis with ICP-MS was presented by Nomizu *et al.* in 2002.[16] The detection was performed with 20 μs time resolution for 1 min in the pulse-counting mode; however, it is stated that the measurement time was limited by the computer hard disc space. Later, ICP-MS became commercially available which allows data acquisition with 100, 50 and 10 μs dwell times. For example, several authors utilized a dwell time as low as 10 μs and highlighted the advantages and disadvantages compared to millisecond time.[49,75,76] In the study by Montaño *et al.*, NP signal extraction from the background was carried out by applying a three time standard deviation (SD) of the background criterion.[49] One limitation of commercially available ICP-MS instrumentation is the fact that the total measurement time with high time resolution is currently limited to minutes. An ideal spICP-MS instrument would be able to operate continuously with microsecond time resolution (hours rather than minutes), without significant dead time, and be able to process the data online. As a contribution from our group to help to get closer to such an ideal system, we presented a DAQ system developed in-house for spICP-MS with 5 μs time resolution and truly continuous data acquisition (Fig. 6).[77] The system allows performing acquisition for any measurement duration (only limited by the hard disk space). It was used for continuous measurements for up to 60 min with the coupling of a separation technique.[10] The obtained data were processed with in-house written software and particle events were extracted on a particle-by particle level by setting defined count thresholds.[77]

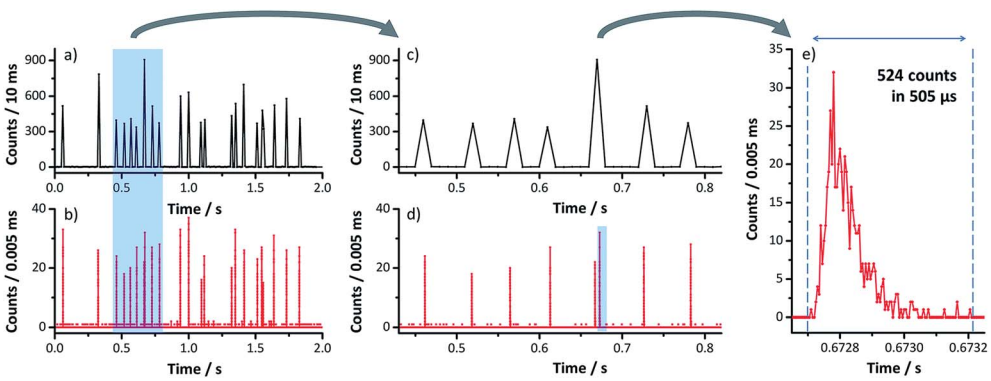

Fig. 6 Representative ICP-MS signal (monitoring m/z $^{197}Au^{+}$) due to 30 nm Au NPs ($C_{NP} = 2.5 \times 10^5$ NP mL^{-1}) acquired simultaneously for 2 s with (a) 10 ms dwell time (vendor software), and (b) 5 μs dwell time (home-built data acquisition system). First zoom level shows several particle events in (c) and (d) for 500 ms (of the highlighted section in a and b). Second zoom level (e) shows the temporal profile of a single particle's ion cloud identified with the home-built data acquisition system in (d). Reproduced from Strenge and Engelhard[77] with permission from the Royal Society of Chemistry.

SF-ICP-MS has also been used with microsecond time resolution (as short as 10 μs).[59,60,63,64] NP identification in the raw data was carried out by determining the peak maxima above a certain threshold.[59,64] Tuoriniemi *et al.* introduced a peak recognition algorithm into an SF-ICP-MS using a 100 μs dwell time based on cluster detection.[60] Another mass analyzer that can be used for fast detection of NPs is an ICP-TOF-MS that can be operated with a speed of up to 30 kHz.[68]

While the majority of spICP-MS studies investigate spherically shaped nanomaterials (or assume a spherical shape), first attempts have been undertaken to distinguish NPs with different shapes and high aspect ratios. For example, microsecond time resolution helped to distinguish spherical NPs from nanorods and to perform dimensional characterization of the NPs based on their ion cloud signal duration.[78] The composition of NPs of gold and silver alloys has also been assessed using profiles of the ion clouds.[79] The detection of silica colloids, which otherwise would require the use of a collision gas to remove polyatomic interference (from nitrogen dimer ions), has been simplified with microsecond time resolution detection.[80]

As reported above, the advent of microsecond time resolution helped to significantly improve the performance of spICP-MS compared to millisecond time resolved data. The number of data points per ion cloud event is improved, the background is divided between adjacent dwells,[76,77] and, thus, the detection of NPs is possible in a wider range of PNCs and in the presence of a higher background and dissolved ion concentrations. However, it should also be noted that the data obtained with microsecond time resolution represent in most of the cases only several counts per dwell time (with 5–10 μs dwell times) and that the normal distribution statistics may not apply to these data anymore. In fact, we suggest that Poisson statistics should be considered in order to differentiate NPs from the background.[81]

2.7 Quantification considerations

The principles of quantification with spICP-MS were described in previous reviews in detail.[6,8,9] Briefly speaking, quantification can be performed using NP standards of the same elemental composition or dissolved standard solutions of the element after taking into account the nebulization efficiency in order to obtain particle size and size distributions with a pneumatic nebulizer. The PNC determination requires a NP standard with the known PNC of the same element, or of a different element, if the same transport and nebulization efficiencies are assumed. The main limitation today is the fact that only a limited variety of the NP standards of different compositions and certified PNCs exist,[9] and difficulties in determination of the nebulization efficiency can occur.[82] Interlaboratory studies have shown that the determination of median particle diameter (2–5% repeatability SD and 15–25% reproducibility SD) is much more repeatable and reproducible compared to the determination of PNC (7–18% repeatability SD and 70–90% reproducibility SD). The lack of stability of the NPs in initial suspensions and different matrices depending on the handling and storage conditions may have a significant contribution to this fact.[82,83] Recently, a metrological study assessing the determination and validation of Au NP size and size distribution was performed.[84] High-resolution scanning electron microscopy (HR-SEM) was used as one of the methods to validate the results obtained with spICP-MS. The two methods show a good agreement with a relative precision of 0.5%. It was emphasized that the NP size characterization provided by their suppliers is not sufficient, and that more characterization is needed if the NPs are intended to be used in research. Alternative methods including the use of a MDG,[30,32,33] isotope dilution,[66,67] and flow injection[85,86] are promising new quantification approaches. However, more studies on the metrology of these methods are required to ensure accurate NP analysis.

The counting stage of the electron multiplier is typically used up to 2×10^6 cps (ref. 27) because there is a detector dead time (on the order of 50 ns)[77] between the acquisitions caused by physical and detector construction limitations. Because NPs result in short but intense ion signals, some of the counts per NP are lost due to the dead time (*e.g.* 6.2% for 40 nm and 24.4% for 60 nm Au NPs).[77] This phenomenon leads to a limited LDR for NP size detection. Liu *et al.* extended the LDR for Au NPs from 10 nm to 70 nm in "highest sensitivity mode" to 200 nm in "less sensitive modes".[54] The approaches that can be used to extend the LDR are based on decreasing the temporal ion signal abundance by the use of low extraction voltage[54] or collision-reaction cells.[54,55] The effect of the plasma conditions on the LDR for Au NPs was investigated by Lee and Chan and 250 nm Au NPs were reportedly outside of the LDR.[87]

The size LODs depend on the sensitivity of the instrument, and an ideal LOD of one atom cannot be achieved nowadays with the current ICP-MS systems. The main reasons are a low nebulization efficiency, low ionization efficiencies of some elements in the argon plasma, and ion transfer into and inside the mass spectrometer. Lee *et al.* calculated the size LODs for 40 elements for an ICP-Q-MS.[70] So far, most of the elements still have LODs well above 10 nm (ref. 6 and 70) and spICP-MS instruments are yet to be developed that can cover the complete nanoscale from 1 nm to 100 nm routinely.

PNC and size LODs are both based on a statistical evaluation of the data; therefore, data processing plays an important role in spICP-MS. For millisecond time resolution, the size LOD is usually determined as $3 \times SD_{BG}$ (SD of the background) or $5 \times SD_{BG}$ above the background.[69,88] Real world samples may have higher size LODs due to a continuous background. If the blank is well known and no NP events are detected, then the PNC LOD was proposed to be three detected NP events by Laborda *et al.*[88] based on the Currie Poisson–Normal approximation ($2.71 + 3.29\sqrt{SD_{BG}}$ for a "well-known" blank). This PNC LOD may need recalculation if some NP events are detected even in blanks. The data obtained with microsecond time resolution usually require even more data processing, because each NP is represented by several data points. Until now there is still no established approach to extract NPs from the raw data, and each developed system utilizes its own algorithm (discussed in the previous chapter). Therefore, there is still a need to develop statistical approaches based on counting statistics for the quantitative extraction of NPs from time-resolved data.

Table 2 Separation methods coupled to spICP-MS for NP analysis

Technique coupled online	Analytes	Nebulizer and spray chamber	Plasma parameters	Dwell time	Separation features	Ref.
CE	10, 20, 30, 40, and 60 nm citrate-coated Au NPs	Microflow nebulizer with a low volume spray chamber	RF power 1500 W, cooling gas 15 L min^{-1}, auxiliary gas 1 L min^{-1}, nebulizer gas 0.8 L min^{-1}, sampling position 7 mm	2 ms	70 mM SDS and 10 mM CAPS in pH 10 buffer	98
CE	20, 40, and 60 nm citrate-coated Ag NPs	Microflow nebulizer with a low volume spray chamber	RF power 1450 W, cooling gas 14 L min^{-1}, auxiliary gas 0.8 L min^{-1}, nebulizer gas 0.8 L min^{-1}, sampling position 3.5 mm	5 μs	60 mM SDS and 10 mM CAPS in pH 10 buffer, online preconcentration	10
CE	20, 40, and 60 nm citrate-coated; 20, 40, and 60 nm PVP-coated; 40 and 60 nm PEG-coated; 40 nm BPEI-coated Ag NPs	Microflow nebulizer with a low volume spray chamber	RF power 1450 W, cooling gas 14 L min^{-1}, auxiliary gas 0.8 L min^{-1}, nebulizer gas 0.8 L min^{-1}, sampling position 3.5 mm	5 μs	60 mM SDS and 10 mM CAPS in pH 10 buffer, online preconcentration, separation of NPs with different coatings	99
ES-DMA	30, 40, 60, 80, and 100 nm Au NPs	n/s	n/s	10 ms	Ammonium acetate was used for electrospray, aggregate detection	96
ES-DMA	CTAB- and citrate-coated Au nanorods (diameters 11.8 to 38.2 nm and aspect ratios 1.8 to 6.9)	n/s	n/s	10 ms	Quantification of the length and diameter of nanorods	97
FFF	40, 60, 80, and 100 nm citrate-coated Ag NPs, 60 nm citrate coated Au NPs, 51 nm Ag core and 21.6 nm SiO_2 shell citrate-coated NPs	Concentric nebulizer with a cyclonic spray chamber	Nebulizer gas 0.88–0.96 L min^{-1}	5 ms	10 kDa regenerated cellulose membrane, 0.02% FL-70 carrier, separation of Au/SiO_2 core/shell NPs from Au NPs	95
FFF	AgPURE® (<20 nm polyoxyethylene fatty acid ester-coated) in food simulants (water, 10% ethanol, and 3% acetic acid) extracted from model films	Concentric nebulizer with a cyclonic spray chamber	RF power 1550 W, cooling gas 14 L min^{-1}, auxiliary gas 0.8 L min^{-1}, nebulizer gas 1 L min^{-1}	5 ms	10 kDa regenerated cellulose membrane, ultrapure water as the mobile phase	100
HDC	30, 60, 80, and 100 nm citrate-coated Au NPs	V-groove nebulizer with a double pass Scott spray chamber	n/s	10 ms	10 mM SDS in pH 11 eluent	94

Table 2 (*Contd.*)

Technique coupled online	Analytes	Nebulizer and spray chamber	Plasma parameters	Dwell time	Separation features	Ref.
HDC	10, 30, 50, 100, and 150, 250 nm citrate-coated Au NPs	PTFE spray chamber	RF power 1400 W, auxiliary gas 0.82 L min^{-1}, nebulizer gas 0.78 L min^{-1}, sampling position 40 mm	5 ms	2 mM Na_2PO_4, 60 mM formaldehyde, 1.8 mM SDS, 3.2 mM Brij L23, and 3.2 mM Triton X-100 in pH 7.5–8 eluent	101
HDC	40 and 80 nm Ag NPs spiked in Milli Q water, WWTP influents and effluents	n/s	n/s	100 μs	1 mM $NaNO_3$, 0.0013% w/w SDS, and 0.0013% w/w Triton X-100 in pH 7.5 eluent	102

Another issue in NP quantification is the differentiation of NPs from the background. The continuous background in ICP-MS may be a result of dissolved ions, natural background, or interference. Bi *et al.* proposed an approach to differentiate NPs from the background with the use of K-means clustering to improve the differentiation of the NPs from the BG compared to the "traditional standard deviation approach".[89] Cornelis and Hassellöv developed an approach for data deconvolution taking into the account the noise components of ICP-MS to differentiate the NPs that are not fully resolved from the background.[90] An approach that utilizes modelling of the background based on the noise components with Monte Carlo simulation was developed for the data obtained with ICP-TOF-MS with 200 Hz resolution.[91] The method allows distinguishing small NPs from the background, and the decision criteria for NP detection were revisited. Alternatively, dissolved ions can be removed with ion exchange resins[92] or the samples can be analyzed after dilutions.[93] Microsecond time resolution helps to distinguish NPs from a continuous background (up to 1 000 000 cps) and quantify both the dissolved ions and NPs.[81]

2.8 Coupling of spICP-MS to separation techniques

A promising approach to obtain more information about mixtures of NPs is the online coupling of spICP-MS to a separation technique. As spICP-MS is used for NP size and size distribution determination, different separation techniques allow obtaining complimentary information. However, the main challenge is that spICP-MS requires the discrete detection of individual NPs while separation techniques will result in a local preconcentration of analytes of a certain type (in a peak), which then elute/migrate together from the column/capillary. Additionally, separation techniques usually require a separation medium (mainly organic compounds) that is introduced into the ICP-MS and may cause matrix effects. Therefore, the combined use of a separation/fractionation technique and spICP-MS requires a careful method development to ensure that:

- The NPs are separated based on their properties but not focused in time to the extent that the detection of single NPs is significantly hindered.
- The organic buffer does not interfere with the NP detection (instrumental parameter optimization).
- A suitable dwell time is chosen.
- The NPs do not undergo size transformations during the separation.
- The best size and PNC LODs are achieved.

An overview of the separation techniques that were coupled online to spICP-MS is presented in Table 2, and the main features are highlighted. The first online coupling of spICP-MS to hydrodynamic chromatography (HDC) was presented by Pergantis *et al.* in 2012, where Au NPs were separated by their size.[94] In 2016, spICP-MS was coupled online to asymmetric field flow fractionation (AF4) to fractionate the NPs by their size and also core–shell NPs (Ag core with a SiO_2 shell) from mono-component NPs (Ag NPs) (Fig. 7).[95] Electrospray-differential mobility analysis (ES-DMA) was also coupled online to spICP-MS.[96] This method allows distinguishing different sizes of NPs, assessing their aggregation,[96] and distinguishing nanorods from spherical NPs.[97] The coupling of capillary electrophoresis (CE) to spICP-MS[98] allows separation of the NPs not only by their size, but also in some cases by their different coatings (Fig. 8).[99] According to Table 2, most of the separation methods utilize surfactants, most commonly sodium dodecyl sulfate (SDS), to enhance the separation of NPs from each other. The coupling of separation techniques online to spICP-MS has the potential to answer non-trivial questions in NP mixtures analysis, where spICP-MS alone does not provide sufficient information.

3 Applications of spICP-MS

There has been a significant increase in the number of published studies that utilize spICP-MS in recent years (Fig. 1) and the majority of these publications are dedicated to applications thereof. Table 1 summarizes the papers that include applications of spICP-MS for the analysis of different samples and

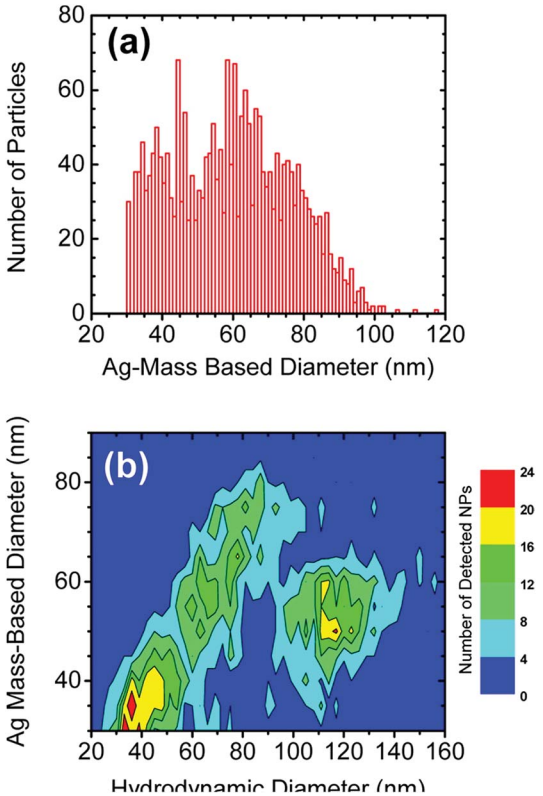

Fig. 7 (a) Size distribution of a mixture containing 40 (1 ng L^{-1}), 60 (2 ng L^{-1}), and 80 nm (6 ng L^{-1}) Ag NPs and Ag–SiO_2 NPs (1 ng Ag per L) obtained using spICP-MS. (b) Contour plot result of an AF4-spICP-MS analysis on a suspension containing 40, 60, and 80 nm Ag NPs (678 ng L^{-1}, 1.39 μg L^{-1}, and 3.73 μg L^{-1}, respectively) and Ag–SiO_2 NPs (624 ng Ag per L). In (a) and (b), the Ag mass concentration ratio of 40, 60, and 80 nm AgNPs, and Ag–SiO_2 NPs was about 1 : 2 : 6 : 1. Reprinted with permission from Huynh *et al.*[95] Copyright 2016 American Chemical Society.

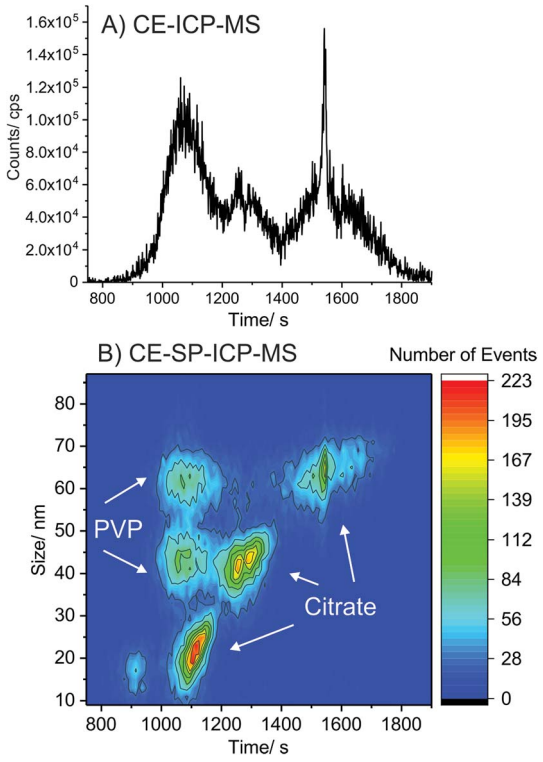

Fig. 8 Comparison of a standard CE-ICP-MS plot (A) and first CE-spICP-MS two-dimensional color map (B) acquired from a complex five-component mixture of different nanomaterials (5 μg L^{-1} citrate-coated 20 nm sized, 35 μg L^{-1} each citrate and PVP-coated 40 nm sized, 100 μg L^{-1} PVP-coated 60 nm sized, and 200 μg L^{-1} citrate-coated 60 nm sized Ag NPs). The analysis was conducted by monitoring at $^{107}Ag^{+}$ with 5 μs dwell time, using 110 s injection and REPSM at 20 kV. Reprinted with permission from Mozhayeva *et al.*[99] Copyright 2017 American Chemical Society.

different matrices (note that fundamental studies on spICP-MS are not included). The studies included in Table 1 are grouped by the analysis matrix and then sorted by the year of publication. Table 1 is a summary of the articles with a short description of the sample preparation and selected instrumental parameters. The reader is advised to check the original publications for more details.

It became apparent when compiling this table that many publications do not include all experimental conditions that the authors of this review consider important for spICP-MS. As discussed above, the combination of RF power, sampling position, and carrier gas flow is crucial for the best spICP-MS performance. The parameters dwell time and measured isotopes are very important as well. Most of the articles state the dwell time that was used for the measurements, with microsecond time resolution (most frequently 0.1 ms dwell time) becoming more widely used in recent years. The majority of the articles do not include the sampling position or injector diameter in the experimental descriptions. Some articles cite their previous studies and do not cite the exact conditions that were used for the study.

The majority of the spICP-MS application papers (Table 1) utilize a method for direct analysis of aqueous media (exposure media, model and real environmental water samples, *etc.*) with or without dilution. Dilution is an effective tool to reduce the matrix load. A filtration step is introduced frequently to avoid clogging of the nebulizer; however, this step may lead to partial losses of NPs due to interactions with the filter membrane materials, even if the NPs are smaller than the membrane pores.[103] Therefore, more research is required to determine suitable filter materials for NPs with different coatings to reduce these interactions or identify membranes that show a somewhat reproducible adsorption behavior. When enzymatic or alkaline digestions are used for more complex matrices (tissue, plants, *etc.*), care must be taken to ensure that the NPs keep their initial state after these procedures. The ultimate goal of any sample preparation step must be a high particle recovery rate and little to no species transformation.

4 Conclusion

The past two decades have witnessed the commercial realization of new and powerful ICP-MS instrumentation and methods, including instruments with faster data acquisition,

enhanced detection power, alternative mass analyzers, off-the-shelf interfaces to couple liquid chromatography, CE, *etc.* to ICP-MS, and novel separation and fractionation methods. While these instruments were successfully used for nanomaterial characterization and the number of published studies of spICP-MS is steadily increasing, there are some remaining challenges that need to be addressed to ultimately reach the top of the nanoparticle peak.

Total consumption microflow nebulizers or droplet generators are attractive due to a high particle transport efficiency. However, microflow nebulizers sometimes suffer from clogging (in the presence of agglomerates or organic matter) and commercially available droplet generators reportedly suffer from a limited day-to-day reproducibility and cannot be coupled to autosamplers in the state in which they are available today. Future research in the area of sample introduction for both stand-alone spICP-MS and when interfaced with separation methods (*e.g.* CE-spICP-MS) is encouraged to address these and other challenges with the ultimate goal of a high-throughput and robust sample introduction system for single particle (and single-cell) ICP-MS. While sample introduction is a potential source of error, sample preparation is often overlooked but may play an even bigger role, especially when particle number concentrations are to be determined. Here, more fundamental studies on potential analyte losses and species transformation (oxidation, release of ions, change of size, and agglomeration) during sampling, storage, and sample preparation are required. For example, a common sample preparation step is filtration to remove unwanted organic matter and larger particle fractions. However, particle losses might occur depending on the particle size and surface coating interaction with the filter material and are often overlooked when particle number concentrations are reported. Similarly to conventional analytical methods, the analyte (particle) recovery should become a parameter that is always reported in future spICP-MS studies.

Based on the publications discussed in this review and from our own findings, we would like to stress that a careful optimization of the plasma conditions and dwell time is required to achieve better NP size detection limits and accurate particle size and number information respectively. In addition, instrumental developments to improve the ion sampling/transfer efficiency in ICP-MS would help to further decrease the size detection limits for single particles and also to gain access to information on NPs of mixed elemental composition and core/shell materials.

While quadrupole-based ICP-MS systems were widely used in past spICP-MS studies, we assume that mass analyzers that provide fast time-resolved and multielement detection such as ICP-TOF-MS will play an important role in this field in the future. However, even the best instrument is worthless if it cannot be calibrated properly, and there is still the lack of appropriate reference materials for calibration. In the future, the field would benefit from more well-characterized and certified nanomaterials to ensure accurate and precise quantification.

It can be concluded that spICP-MS is a very useful method for NP analysis today but there is still room for fundamental studies, instrumental improvements, and methodological advances to come closer to what would be an ideal method for nanomaterial characterization.

Conflicts of interest

There are no conflicts to declare. The manuscript was written through contributions of all authors. All authors have given approval to the final version of the manuscript. The authors declare no competing financial interest.

Note added after first publication

This article replaces the version published on 5th August 2019, which contained errors in Table 1.

List of abbreviations

AF4	asymmetrical flow field-flow fractionation
BPEI	branched polyethyleneimine
BSA	bovine serum albumin
CAPS	3-cyclohexylamoniuopropanesulfonic acid
CE	capillary electrophoresis
CIGS	copper indium gallium selenide cells
CNT	carbon nanotube
CPE	cloud point extraction
CTAB	cetyltrimethylammonium bromide
DAQ	data acquisition
DMEM	Dulbecco's modified eagle medium
EPA	Environmental Protection Agency
ESD	equivalent spherical diameter
ES-DMA	electrospray-differential mobility analysis
FFF	field flow fractionation
HDC	hydrodynamic chromatography
HR-SEM	high-resolution scanning electron microscopy
ICP-Q-MS	single quadrupole ICP-MS
IEC	ion-exchange column
KED	kinetic energy discrimination
LA	laser ablation
LDR	linear dynamic range
LOD	detection limit
m/z	mass-to-charge ratio
MA	multielement analysis
MC	multi-collector
MDG	microdroplet generator
MOPS	3-morpholinopropane-1-sulfonic acid
n/a	not applicable
n/s	not specified
NOM	natural organic matter
NP	nanoparticle
OECD	The Organization for Economic Co-operation and Development
OES	optical emission spectrometry
OPV	organic photovoltaic cells
PBS	phosphate buffered saline

PEG	polyethylene glycol
PFA	perfluoroalkoxy alkane
PNC	particle number concentration
PTFE	polytetrafluoroethylene
PVA	polyvinyl alcohol
PVP	polyvinylpyrrolidone
Q	quadrupole
QQQ	triple quadrupole
RF	radio frequency
SD	standard deviation
SDS	sodium dodecyl sulfate
SEM	secondary electron multiplier
SF	sector field
spICP-MS	single particle inductively coupled plasma mass spectrometry
TAP	tris-acetate-phosphate
TMAH	tetramethylammonium hydroxide
TOF	time-of-flight
TQ	triple quadrupole
TSPP	tetrasodium pyrophosphate
WWTP	waste water treatment plant

Acknowledgements

We acknowledge the House of Young Talents of the University of Siegen for providing funding for Darya Mozhayeva.

References

1 G. M. Hieftje, Howard Malmstadt – Toward the ideal, *Spectrochim. Acta, Part B*, 2006, **61**, 597–598.
2 R. P. Feynman, There's plenty of room at the bottom, *Eng. Sci.*, 1960, **23**, 22–36.
3 M. Faraday, Experimental relations of gold (and other metals) to light, *Philos. Trans. R. Soc. London*, 1857, **147**, 145–181.
4 F. R. S. Thomas Graham, Liquid diffusion applied to analysis, *Philos. Trans. R. Soc. London*, 1861, **151**, 183–224.
5 C. Degueldre and P. Y. Favarger, Colloid analysis by single particle inductively coupled plasma-mass spectroscopy: a feasibility study, *Colloids Surf., A*, 2003, **217**, 137–142.
6 F. Laborda, E. Bolea and J. Jiménez-Lamana, Single particle inductively coupled plasma mass spectrometry: a powerful tool for nanoanalysis, *Anal. Chem.*, 2014, **86**, 2270–2278.
7 F. Laborda, E. Bolea and J. Jiménez-Lamana, Single particle inductively coupled plasma mass spectrometry for the analysis of inorganic engineered nanoparticles in environmental samples, *Trends Environ. Anal. Chem.*, 2016, **9**, 15–23.
8 M. D. Montaño, J. W. Olesik, A. G. Barber, K. Challis and J. F. Ranville, Single particle ICP-MS: advances toward routine analysis of nanomaterials, *Anal. Bioanal. Chem.*, 2016, **408**, 5053–5074.
9 B. Meermann and V. Nischwitz, ICP-MS for the analysis at the nanoscale – a tutorial review, *J. Anal. At. Spectrom.*, 2018, **33**, 1432–1468.
10 D. Mozhayeva, I. Strenge and C. Engelhard, Implementation of online preconcentration and microsecond time resolution to capillary electrophoresis single particle inductively coupled plasma mass spectrometry (CE-SP-ICP-MS) and its application in silver nanoparticle analysis, *Anal. Chem.*, 2017, **89**, 7152–7159.
11 H. Kawaguchi, N. Fukasawa and A. Mizuike, Investigation of airborne particles by inductively coupled plasma emission-spectrometry calibrated with monodisperse aerosols, *Spectrochim. Acta, Part B*, 1986, **41**, 1277–1286.
12 U. K. Bochert and W. Dannecker, On-line aerosol analysis by atomic emission spectroscopy, *J. Aerosol Sci.*, 1989, **20**, 1525–1528.
13 T. Nomizu, S. Kaneco, T. Tanaka, T. Yamamoto and H. Kawaguchi, Determination of femto-gram amounts of zinc and lead in individual airborne particles by inductively coupled plasma mass spectrometry with direct air-sample introduction, *Anal. Sci.*, 1993, **9**, 843–846.
14 S. Kaneco, T. Nomizu, T. Tanaka, N. Mizutani and H. Kawaguchi, Optimization of operating conditions in individual airborne particle analysis by inductively coupled plasma mass spectrometry, *Anal. Sci.*, 1995, **11**, 835–840.
15 T. Nomizu, H. Nakashima, Y. Hotta, T. Tanaka and H. Kawaguchi, Simultaneous measurement of the elemental content and size of airborne particles by inductively coupled plasma emission spectrometry combined with the laser light-scattering method, *Anal. Sci.*, 1992, **8**, 527–531.
16 T. Nomizu, H. Hayashi, N. Hoshino, T. Tanaka, H. Kawaguchi, K. Kitagawa and S. Kaneco, Determination of zinc in individual airborne particles by inductively coupled plasma mass spectrometry with digital signal processing, *J. Anal. At. Spectrom.*, 2002, **17**, 592–595.
17 M. Thompson, C. D. Flint, S. Chenery and K. Knight, Time resolved system for the analysis of particles in the inductively coupled plasma - preliminary studies, *J. Anal. At. Spectrom.*, 1992, **7**, 1099–1102.
18 K. Knight, S. Chenery, S. W. Zochowski, M. Thompson and C. D. Flint, Time-resolved signals from particles injected into the inductively coupled plasma, *J. Anal. At. Spectrom.*, 1996, **11**, 53–56.
19 C. Degueldre, P. Y. Favarger and C. Bitea, Zirconia colloid analysis by single particle inductively coupled plasma–mass spectrometry, *Anal. Chim. Acta*, 2004, **518**, 137–142.
20 C. Degueldre and P. Y. Favarger, Thorium colloid analysis by single particle inductively coupled plasma-mass spectrometry, *Talanta*, 2004, **62**, 1051–1054.
21 C. Degueldre, P. Y. Favarger, R. Rosse and S. Wold, Uranium colloid analysis by single particle inductively coupled plasma-mass spectrometry, *Talanta*, 2006, **68**, 623–628.
22 C. Degueldre, P. Y. Favarger and S. Wold, Gold colloid analysis by inductively coupled plasma-mass spectrometry in a single particle mode, *Anal. Chim. Acta*, 2006, **555**, 263–268.

23 G. M. Hieftje, *presented in part at the European Winter Conference on Plasma Spectrochemistry*, Sankt Anton am Arlberg, Austria, 2017.
24 G. M. Hieftje, *presented in part at the Winter Conference on Plasma Spectrochemistry*, Amelia Island, FL, U.S.A., 2018.
25 F. Laborda, E. Bolea, G. Cepriá, M. T. Gómez, M. S. Jiménez, J. Pérez-Arantegui and J. R. Castillo, Detection, characterization and quantification of inorganic engineered nanomaterials: a review of techniques and methodological approaches for the analysis of complex samples, *Anal. Chim. Acta*, 2016, **904**, 10–32.
26 I. De la Calle, M. Menta and F. Séby, Current trends and challenges in sample preparation for metallic nanoparticles analysis in daily products and environmental samples: a review, *Spectrochim. Acta, Part B*, 2016, **125**, 66–96.
27 J. W. Olesik and P. J. Gray, Considerations for measurement of individual nanoparticles or microparticles by ICP-MS: determination of the number of particles and the analyte mass in each particle, *J. Anal. At. Spectrom.*, 2012, **27**, 1143–1155.
28 S. I. Miyashita, H. Mitsuhashi, S. I. Fujii, A. Takatsu, K. Inagaki and T. Fujimoto, High transport efficiency of nanoparticles through a total-consumption sample introduction system and its beneficial application for particle size evaluation in single-particle ICP-MS, *Anal. Bioanal. Chem.*, 2017, **409**, 1531–1545.
29 S. Gschwind, L. Flamigni, J. Koch, O. Borovinskaya, S. Groh, K. Niemax and D. Günther, Capabilities of inductively coupled plasma mass spectrometry for the detection of nanoparticles carried by monodisperse microdroplets, *J. Anal. At. Spectrom.*, 2011, **26**, 1166–1174.
30 S. Gschwind, H. Hagendorfer, D. A. Frick and D. Günther, Mass quantification of nanoparticles by single droplet calibration using inductively coupled plasma mass spectrometry, *Anal. Chem.*, 2013, **85**, 5875–5883.
31 L. Hendriks, B. Ramkorun-Schmidt, A. Gundlach-Graham, J. Koch, R. N. Grass, N. Jakubowski and D. Günther, Single-particle ICP-MS with online microdroplet calibration: toward matrix independent nanoparticle sizing, *J. Anal. At. Spectrom.*, 2019, **34**, 716–728.
32 B. Ramkorun-Schmidt, S. A. Pergantis, D. Esteban-Fernández, N. Jakubowski and D. Günther, Investigation of a combined microdroplet generator and pneumatic nebulization system for quantitative determination of metal-containing nanoparticles using ICPMS, *Anal. Chem.*, 2015, **87**, 8687–86894.
33 S. Gschwind, M. d. L. A. Montes and D. Günther, Comparison of sp-ICP-MS and MDG-ICP-MS for the determination of particle number concentration, *Anal. Bioanal. Chem.*, 2015, **407**, 4035–4044.
34 B. Franze, I. Strenge and C. Engelhard, Single particle inductively coupled plasma mass spectrometry: evaluation of three different pneumatic and piezo-based sample introduction systems for the characterization of silver nanoparticles, *J. Anal. At. Spectrom.*, 2012, **27**, 1074–1083.
35 D. Metarapi, M. Sala, K. Vogel-Mikus, V. S. Selih and J. T. van Elteren, Nanoparticle analysis in biomaterials using laser ablation-single particle-inductively coupled plasma mass spectrometry, *Anal. Chem.*, 2019, **91**, 6200–6205.
36 M. Guillong and D. Günther, Effect of particle size distribution on ICP-induced elemental fractionation in laser ablation-inductively coupled plasma-mass spectrometry, *J. Anal. At. Spectrom.*, 2002, **17**, 831–837.
37 M. Guillong, H.-R. Kuhn and D. Günther, Application of a particle separation device to reduce inductively coupled plasma-enhanced elemental fractionation in laser ablation-inductively coupled plasma-mass spectrometry, *Spectrochim. Acta, Part B*, 2003, **58**, 211–220.
38 K. S. Ho, W. W. Lee and W. T. Chan, Effects of ionization potential of an element and boiling point of the corresponding oxide on the sensitivity of ICP-MS, *J. Anal. At. Spectrom.*, 2015, **30**, 2066–2073.
39 S. Groh, C. C. Garcia, A. Murtazin, V. Horvatic and K. Niemax, Local effects of atomizing analyte droplets on the plasma parameters of the inductively coupled plasma, *Spectrochim. Acta, Part B*, 2009, **64**, 247–254.
40 A. Murtazin, S. Groh and K. Niemax, Investigation of sample introduction- and plasma-related matrix effects in inductively coupled plasma spectrometry applying single analyte droplet and particle injection, *Spectrochim. Acta, Part B*, 2012, **67**, 3–16.
41 K. S. Ho, K. O. Lui, K. H. Lee and W. T. Chan, Considerations of particle vaporization and analyte diffusion in single-particle inductively coupled plasma-mass spectrometry, *Spectrochim. Acta, Part B*, 2013, **89**, 30–39.
42 O. Borovinskaya, M. Aghaei, L. Flamigni, B. Hattendorf, M. Tanner, A. Bogaerts and D. Günther, Diffusion- and velocity-driven spatial separation of analytes from single droplets entering an ICP off-axis, *J. Anal. At. Spectrom.*, 2014, **29**, 262–271.
43 M. Aghaei and A. Bogaerts, Particle transport through an inductively coupled plasma torch: elemental droplet evaporation, *J. Anal. At. Spectrom.*, 2016, **31**, 631–641.
44 G. C. Y. Chan and G. M. Hieftje, Local cooling, plasma reheating and thermal pinching induced by single aerosol droplets injected into an inductively coupled plasma, *Spectrochim. Acta, Part B*, 2016, **121**, 55–66.
45 I. Kálomista, A. Kéri and G. Galbács, Optimization of plasma sampling depth and aerosol gas flow rates for single particle inductively coupled plasma mass spectrometry analysis, *Talanta*, 2017, **172**, 147–154.
46 K. H. Chun, H. Zhang and W. T. Chan, Double-viewing-position single-particle inductively coupled plasma-atomic emission spectrometry for the selection of ICP sampling position in SP-ICP measurements, *Anal. Sci.*, 2018, **34**, 711–717.
47 H. Niu and R. S. Houk, Fundamental aspects of ion extraction in inductively coupled plasma mass spectrometry, *Spectrochim. Acta, Part B*, 1996, **51**, 779–815.

48 S. J. Hill, A. Fisher and M. Liezers, in *Inductively Coupled Plasma Mass Spectrometry Handbook*, ed. S. M. Nelms, Blackwell Publishing Ltd, Oxford, UK, 2005, pp. 1–25.
49 M. D. Montaño, H. R. Badiei, S. Bazargan and J. F. Ranville, Improvements in the detection and characterization of engineered nanoparticles using spICP-MS with microsecond dwell times, *Environ. Sci.: Nano*, 2014, **1**, 338–346.
50 T. W. May and R. H. Wiedmeyer, A table of polyatomic interferences in ICP-MS, *Atom. Spectrosc.*, 1998, **19**, 150–155.
51 F. Laborda, J. Medrano and J. R. Castillo, Quality of quantitative and semiquantitative results in inductively coupled plasma mass spectrometry, *J. Anal. At. Spectrom.*, 2001, **16**, 732–738.
52 A. T. Ince, J. G. Williams and A. L. Gray, Noise in inductively-coupled plasma-mass spectrometry - some preliminary measurements, *J. Anal. At. Spectrom.*, 1993, **8**, 899–903.
53 F. Laborda, J. Jiménez-Lamana, E. Bolea and J. R. Castillo, Selective identification, characterization and determination of dissolved silver(I) and silver nanoparticles based on single particle detection by inductively coupled plasma mass spectrometry, *J. Anal. At. Spectrom.*, 2011, **26**, 1362–1371.
54 J. Liu, K. E. Murphy, R. I. MacCuspie and M. R. Winchester, Capabilities of single particle inductively coupled plasma mass spectrometry for the size measurement of nanoparticles: a case study on gold nanoparticles, *Anal. Chem.*, 2014, **86**, 3405–3414.
55 L. A. Rush, M. C. Endres, M. Liezers, J. D. Ward, G. C. Eiden and A. M. Duffin, Collisional dampening for improved quantification in single particle inductively coupled plasma mass spectrometry, *Talanta*, 2018, **189**, 268–273.
56 E. Bolea-Fernandez, D. Leite, A. Rua-Ibarz, L. Balcaen, M. Aramendia, M. Resano and F. Vanhaecke, Characterization of SiO_2 nanoparticles by single particle-inductively coupled plasma-tandem mass spectrometry (SP-ICP-MS/MS), *J. Anal. At. Spectrom.*, 2017, **32**, 2140–2152.
57 S. Candás-Zapico, D. J. Kutscher, M. Montes-Bayón and J. Bettmer, Single particle analysis of TiO_2 in candy products using triple quadrupole ICP-MS, *Talanta*, 2018, **180**, 309–315.
58 M. Tharaud, A. P. Gondikas, M. F. Benedetti, F. von der Kammer, T. Hofmann and G. Cornelis, TiO_2 nanomaterial detection in calcium rich matrices by spICPMS. A matter of resolution and treatment, *J. Anal. At. Spectrom.*, 2017, **32**, 1400–1411.
59 P. Shaw and A. Donard, Nano-particle analysis using dwell times between 10 μs and 70 μs with an upper counting limit of greater than 3×10^7 cps and a gold nanoparticle detection limit of less than 10 nm diameter, *J. Anal. At. Spectrom.*, 2016, **31**, 1234–1242.
60 J. Tuoriniemi, G. Cornelis and M. Hassellöv, A new peak recognition algorithm for detection of ultra-small nanoparticles by single particle ICP-MS using rapid time resolved data acquisition on a sector-field mass spectrometer, *J. Anal. At. Spectrom.*, 2015, **30**, 1723–1729.
61 J. Tuoriniemi, G. Cornelis and M. Hassellöv, Improving the accuracy of single particle ICPMS for measurement of size distributions and number concentrations of nanoparticles by determining analyte partitioning during nebulisation, *J. Anal. At. Spectrom.*, 2014, **29**, 743–752.
62 J. Tuoriniemi, M. D. Jurgens, M. Hassellöv and G. Cornelis, Size dependence of silver nanoparticle removal in a wastewater treatment plant mesocosm measured by FAST single particle ICP-MS, *Environ. Sci.: Nano*, 2017, **4**, 1189–1197.
63 A. J. Managh, D. N. Douglas, K. M. Cowen, H. J. Reid and B. L. Sharp, Acquisition of fast transient signals in ICP-MS with enhanced time resolution, *J. Anal. At. Spectrom.*, 2016, **31**, 1688–1692.
64 K. Newman, C. Metcalfe, J. Martin, H. Hintelmann, P. Shaw and A. Donard, Improved single particle ICP-MS characterization of silver nanoparticles at environmentally relevant concentrations, *J. Anal. At. Spectrom.*, 2016, **31**, 2069–2077.
65 S. Yongyang, W. Wei, L. Zhiming, D. Hu, Z. Guoqing, X. Jiang and R. Xiangjun, Direct detection and isotope analysis of individual particles in suspension by single particle mode MC-ICP-MS for nuclear safety, *J. Anal. At. Spectrom.*, 2015, **30**, 1184–1190.
66 L. Telgmann, C. D. Metcalfe and H. Hintelmann, Rapid size characterization of silver nanoparticles by single particle ICP-MS and isotope dilution, *J. Anal. At. Spectrom.*, 2014, **29**, 1265–1272.
67 C. A. Sötebier, D. J. Kutscher, L. Rottmann, N. Jakubowski, U. Panne and J. Bettmer, Combination of single particle ICP-QMS and isotope dilution analysis for the determination of size, particle number and number size distribution of silver nanoparticles, *J. Anal. At. Spectrom.*, 2016, **31**, 2045–2052.
68 O. Borovinskaya, B. Hattendorf, M. Tanner, S. Gschwind and D. Günther, A prototype of a new inductively coupled plasma time-of-flight mass spectrometer providing temporally resolved, multi-element detection of short signals generated by single particles and droplets, *J. Anal. At. Spectrom.*, 2013, **28**, 226–233.
69 J. Tuoriniemi, G. Cornelis and M. Hassellöv, Size discrimination and detection capabilities of single-particle ICPMS for environmental analysis of silver nanoparticles, *Anal. Chem.*, 2012, **84**, 3965–3972.
70 S. Lee, X. Bi, R. B. Reed, J. F. Ranville, P. Herckes and P. Westerhoff, Nanoparticle size detection limits by single particle ICP-MS for 40 elements, *Environ. Sci. Technol.*, 2014, **48**, 10291–10300.
71 O. Borovinskaya, S. Gschwind, B. Hattendorf, M. Tanner and D. Günther, Simultaneous mass quantification of nanoparticles of different composition in a mixture by microdroplet generator-ICPTOFMS, *Anal. Chem.*, 2014, **86**, 8142–8148.
72 A. Praetorius, A. Gundlach-Graham, E. Goldberg, W. Fabienke, J. Navratilova, A. Gondikas, R. Kaegi,

D. Günther, T. Hofmann and F. von der Kammer, Single-particle multi-element fingerprinting (spMEF) using inductively-coupled plasma time-of-flight mass spectrometry (ICP-TOFMS) to identify engineered nanoparticles against the elevated natural background in soils, *Environ. Sci.: Nano*, 2017, **4**, 307–314.

73 A. Gondikas, F. von der Kammer, R. Kaegi, O. Borovinskaya, E. Neubauer, J. Navratilova, A. Praetorius, G. Cornelis and T. Hofmann, Where is the nano? Analytical approaches for the detection and quantification of TiO_2 engineered nanoparticles in surface waters, *Environ. Sci.: Nano*, 2018, **5**, 313–326.

74 S. Naasz, S. Weigel, O. Borovinskaya, A. Serva, C. Cascio, A. K. Undas, F. C. Simeone, H. J. P. Marvin and R. J. B. Peters, Multi-element analysis of single nanoparticles by ICP-MS using quadrupole and time-of-flight technologies, *J. Anal. At. Spectrom.*, 2018, **33**, 835–845.

75 A. Hineman and C. Stephan, Effect of dwell time on single particle inductively coupled plasma mass spectrometry data acquisition quality, *J. Anal. At. Spectrom.*, 2014, **29**, 1252–1257.

76 I. Abad-Álvaro, E. Pena-Vázquez, E. Bolea, P. Bermejo-Barrera, J. R. Castillo and F. Laborda, Evaluation of number concentration quantification by single-particle inductively coupled plasma mass spectrometry: microsecond vs. millisecond dwell times, *Anal. Bioanal. Chem.*, 2016, **408**, 5089–5097.

77 I. Strenge and C. Engelhard, Capabilities of fast data acquisition with microsecond time resolution in inductively coupled plasma mass spectrometry and identification of signal artifacts from millisecond dwell times during detection of single gold nanoparticles, *J. Anal. At. Spectrom.*, 2016, **31**, 135–144.

78 I. Kálomista, A. Kéri, D. Ungor, E. Csapó, I. Dékány, T. Prohaska and G. Galbács, Dimensional characterization of gold nanorods by combining millisecond and microsecond temporal resolution single particle ICP-MS measurements, *J. Anal. At. Spectrom.*, 2017, **32**, 2455–2462.

79 A. Kéri, I. Kálomista, D. Ungor, A. Bélteki, E. Csapó, I. Dékány, T. Prohaska and G. Galbács, Determination of the structure and composition of Au-Ag bimetallic spherical nanoparticles using single particle ICP-MS measurements performed with normal and high temporal resolution, *Talanta*, 2018, **179**, 193–199.

80 M. D. Montaño, B. J. Majestic, A. K. Jamting, P. Westerhoff and J. F. Ranville, Methods for the detection and characterization of silica colloids by microsecond spICP-MS, *Anal. Chem.*, 2016, **88**, 4733–4741.

81 D. Mozhayeva and C. Engelhard, A quantitative nanoparticle extraction method for microsecond time resolved single-particle ICP-MS data in the presence of a high background, *J. Anal. At. Spectrom.*, 2019, DOI: 10.1039/c9ja00042a.

82 S. Weigel, R. Peters, K. Loeschner, R. Grombe and T. P. J. Linsinger, Results of an interlaboratory method performance study for the size determination and quantification of silver nanoparticles in chicken meat by single-particle inductively coupled plasma mass spectrometry (sp-ICP-MS), *Anal. Bioanal. Chem.*, 2017, **409**, 4839–4848.

83 T. P. Linsinger, R. Peters and S. Weigel, International interlaboratory study for sizing and quantification of Ag nanoparticles in food simulants by single-particle ICPMS, *Anal. Bioanal. Chem.*, 2014, **406**, 3835–3843.

84 A. R. Montoro Bustos, K. P. Purushotham, A. Possolo, N. Farkas, A. E. Vladar, K. E. Murphy and M. R. Winchester, Validation of single particle ICP-MS for routine measurements of nanoparticle size and number size distribution, *Anal. Chem.*, 2018, **90**, 14376–14386.

85 R. P. Lamsal, G. Jerkiewicz and D. Beauchemin, Flow injection single particle inductively coupled plasma mass spectrometry: an original simple approach for the characterization of metal-based nanoparticles, *Anal. Chem.*, 2016, **88**, 10552–10558.

86 C. Toncelli, K. Mylona, M. Tsapakis and S. A. Pergantis, Flow injection with on-line dilution and single particle inductively coupled plasma – mass spectrometry for monitoring silver nanoparticles in seawater and in marine microorganisms, *J. Anal. At. Spectrom.*, 2016, **31**, 1430–1439.

87 W. W. Lee and W. T. Chan, Calibration of single-particle inductively coupled plasma-mass spectrometry (SP-ICP-MS), *J. Anal. At. Spectrom.*, 2015, **30**, 1245–1254.

88 F. Laborda, J. Jiménez-Lamana, E. Bolea and J. R. Castillo, Critical considerations for the determination of nanoparticle number concentrations, size and number size distributions by single particle ICP-MS, *J. Anal. At. Spectrom.*, 2013, **28**, 1220–1232.

89 X. Y. Bi, S. Lee, J. F. Ranville, P. Sattigeri, A. Spanias, P. Herckes and P. Westerhoff, Quantitative resolution of nanoparticle sizes using single particle inductively coupled plasma mass spectrometry with the K-means clustering algorithm, *J. Anal. At. Spectrom.*, 2014, **29**, 1630–1639.

90 G. Cornelis and M. Hassellöv, A signal deconvolution method to discriminate smaller nanoparticles in single particle ICP-MS, *J. Anal. At. Spectrom.*, 2014, **29**, 134–144.

91 A. Gundlach-Graham, L. Hendriks, K. Mehrabi and D. Günther, Monte Carlo simulation of low-count signals in time-of-flight mass spectrometry and its application to single-particle detection, *Anal. Chem.*, 2018, **90**, 11847–11855.

92 M. Hadioui, C. Peyrot and K. J. Wilkinson, Improvements to single particle ICPMS by the online coupling of ion exchange resins, *Anal. Chem.*, 2014, **86**, 4668–4674.

93 D. M. Schwertfeger, J. R. Velicogna, A. H. Jesmer, R. P. Scroggins and J. I. Princz, Single particle-inductively coupled plasma mass spectroscopy analysis of metallic nanoparticles in environmental samples with large dissolved analyte fractions, *Anal. Chem.*, 2016, **88**, 9908–9914.

94 S. A. Pergantis, T. L. Jones-Lepp and E. M. Heithmar, Hydrodynamic chromatography online with single particle-inductively coupled plasma mass spectrometry for

ultratrace detection of metal-containing nanoparticles, *Anal. Chem.*, 2012, **84**, 6454–6462.

95 K. A. Huynh, E. Siska, E. Heithmar, S. Tadjiki and S. A. Pergantis, Detection and quantification of silver nanoparticles at environmentally relevant concentrations using asymmetric flow field-flow fractionation online with single particle inductively coupled plasma mass spectrometry, *Anal. Chem.*, 2016, **88**, 4909–4916.

96 J. Tan, J. Liu, M. Li, H. El Hadri, V. A. Hackley and M. R. Zachariah, Electrospray-differential mobility hyphenated with single particle inductively coupled plasma mass spectrometry for characterization of nanoparticles and their aggregates, *Anal. Chem.*, 2016, **88**, 8548–8555.

97 J. Tan, Y. Yang, H. El Hadri, M. Li, V. A. Hackley and M. R. Zachariah, Fast quantification of nanorod geometry by DMA-spICP-MS, *Analyst*, 2019, **144**, 2275–2283.

98 B. Franze, I. Strenge and C. Engelhard, Separation and detection of gold nanoparticles with capillary electrophoresis and ICP-MS in single particle mode (CE-SP-ICP-MS), *J. Anal. At. Spectrom.*, 2017, **32**, 1481–1489.

99 D. Mozhayeva and C. Engelhard, Separation of silver nanoparticles with different coatings by capillary electrophoresis coupled to ICP-MS in single particle mode, *Anal. Chem.*, 2017, **89**, 9767–9774.

100 B. Hetzer, A. Burcza, V. Graf, E. Walz and R. Greiner, Online-coupling of AF^4 and single particle-ICP-MS as an analytical approach for the selective detection of nanosilver release from model food packaging films into food simulants, *Food Control*, 2017, **80**, 113–124.

101 D. Rakcheev, A. Philippe and G. E. Schaumann, Hydrodynamic chromatography coupled with single particle-inductively coupled plasma mass spectrometry for investigating nanoparticles agglomerates, *Anal. Chem.*, 2013, **85**, 10643–10647.

102 K. Proulx, M. Hadioui and K. J. Wilkinson, Separation, detection and characterization of nanomaterials in municipal wastewaters using hydrodynamic chromatography coupled to ICPMS and single particle ICPMS, *Anal. Bioanal. Chem.*, 2016, **408**, 5147–5155.

103 Y. Yang, C. L. Long, H. P. Li, Q. Wang and Z. G. Yang, Analysis of silver and gold nanoparticles in environmental water using single particle-inductively coupled plasma-mass spectrometry, *Sci. Total Environ.*, 2016, **563–564**, 996–1007.

104 M. van der Zande, R. J. Vandebriel, E. Van Doren, E. Kramer, Z. Herrera Rivera, C. S. Serrano-Rojero, E. R. Gremmer, J. Mast, R. J. Peters, P. C. Hollman, P. J. Hendriksen, H. J. Marvin, A. A. Peijnenburg and H. Bouwmeester, Distribution, elimination, and toxicity of silver nanoparticles and silver ions in rats after 28-day oral exposure, *ACS Nano*, 2012, **6**, 7427–7442.

105 J. G. Coleman, A. J. Kennedy, A. J. Bednar, J. F. Ranville, J. G. Laird, A. R. Harmon, C. A. Hayes, E. P. Gray, C. P. Higgins, G. Lotufo and J. A. Steevens, Comparing the effects of nanosilver size and coating variations on bioavailability, internalization, and elimination, using Lumbriculus variegatus, *Environ. Toxicol. Chem.*, 2013, **32**, 2069–2077.

106 E. P. Gray, J. G. Coleman, A. J. Bednar, A. J. Kennedy, J. F. Ranville and C. P. Higgins, Extraction and analysis of silver and gold nanoparticles from biological tissues using single particle inductively coupled plasma mass spectrometry, *Environ. Sci. Technol.*, 2013, **47**, 14315–14323.

107 L. D. Scanlan, R. B. Reed, A. V. Loguinov, P. Antczak, A. Tagmount, S. Aloni, D. T. Nowinski, P. Luong, C. Tran, N. Karunaratne, D. Pham, X. X. Lin, F. Falciani, C. P. Higgins, J. F. Ranville, C. D. Vulpe and B. Gilbert, Silver nanowire exposure results in internalization and toxicity to *Daphnia magna*, *ACS Nano*, 2013, **7**, 10681–10694.

108 K. Loeschner, M. S. Brabrand, J. J. Sloth and E. H. Larsen, Use of alkaline or enzymatic sample pretreatment prior to characterization of gold nanoparticles in animal tissue by single-particle ICPMS, *Anal. Bioanal. Chem.*, 2014, **406**, 3845–3851.

109 R. J. Peters, Z. H. Rivera, G. van Bemmel, H. J. Marvin, S. Weigel and H. Bouwmeester, Development and validation of single particle ICP-MS for sizing and quantitative determination of nano-silver in chicken meat, *Anal. Bioanal. Chem.*, 2014, **406**, 3875–3885.

110 R. Tassinari, F. Cubadda, G. Moracci, F. Aureli, M. D'Amato, M. Valeri, B. De Berardis, A. Raggi, A. Mantovani, D. Passeri, M. Rossi and F. Maranghi, Oral, short-term exposure to titanium dioxide nanoparticles in Sprague-Dawley rat: focus on reproductive and endocrine systems and spleen, *Nanotoxicology*, 2014, **8**, 654–662.

111 S. Makama, R. Peters, A. Undas and N. W. van den Brink, A novel method for the quantification, characterisation and speciation of silver nanoparticles in earthworms exposed in soil, *Environ. Chem.*, 2015, **12**, 643–651.

112 R. Grombe, G. Allmaier, J. Charoud-Got, A. Dudkiewicz, H. Emteborg, T. Hofmann, E. H. Larsen, A. Lehner, M. Llinàs, K. Loeschner, K. Mølhave, R. J. Peters, J. Seghers, C. Solans, F. von der Kammer, S. Wagner, S. Weigel and T. P. J. Linsinger, Feasibility of the development of reference materials for the detection of Ag nanoparticles in food: neat dispersions and spiked chicken meat, *Accredit. Qual. Assur.*, 2015, **20**, 3–16.

113 L. Campagnolo, M. Massimiani, L. Vecchione, D. Piccirilli, N. Toschi, A. Magrini, E. Bonanno, M. Scimeca, L. Castagnozzi, G. Buonanno, L. Stabile, F. Cubadda, F. Aureli, P. H. Fokkens, W. G. Kreyling, F. R. Cassee and A. Pietroiusti, Silver nanoparticles inhaled during pregnancy reach and affect the placenta and the foetus, *Nanotoxicology*, 2017, **11**, 687–698.

114 F. Gallocchio, G. Biancotto, V. Cibin, C. Losasso, S. Belluco, R. Peters, G. van Bemmel, C. Cascio, S. Weigel, P. Tromp, F. Gobbo, S. Catania and A. Ricci, Transfer study of silver nanoparticles in poultry production, *J. Agric. Food Chem.*, 2017, **65**, 3767–3774.

115 M. E. Johnson, S. K. Hanna, A. R. Montoro Bustos, C. M. Sims, L. C. Elliott, A. Lingayat, A. C. Johnston, B. Nikoobakht, J. T. Elliott, R. D. Holbrook, K. C. Scott, K. E. Murphy, E. J. Petersen, L. L. Yu and B. C. Nelson,

Separation, sizing, and quantitation of engineered nanoparticles in an organism model using inductively coupled plasma mass spectrometry and image analysis, *ACS Nano*, 2017, **11**, 526–540.

116 B. Kollander, F. Widemo, E. Agren, E. H. Larsen and K. Loeschner, Detection of lead nanoparticles in game meat by single particle ICP-MS following use of lead-containing bullets, *Anal. Bioanal. Chem.*, 2017, **409**, 1877–1885.

117 K. Ramos, L. Ramos and M. M. Gómez-Gómez, Simultaneous characterisation of silver nanoparticles and determination of dissolved silver in chicken meat subjected to in vitro human gastrointestinal digestion using single particle inductively coupled plasma mass spectrometry, *Food Chem.*, 2017, **221**, 822–828.

118 Q. Li, Z. Wang, J. Mo, G. Zhang, Y. Chen and C. Huang, Imaging gold nanoparticles in mouse liver by laser ablation inductively coupled plasma mass spectrometry, *Sci. Rep.*, 2017, **7**, 2965.

119 J. Modrzynska, T. Berthing, G. Ravn-Haren, K. Kling, A. Mortensen, R. R. Rasmussen, E. H. Larsen, A. T. Saber, U. Vogel and K. Loeschner, *In vivo*-induced size transformation of cerium oxide nanoparticles in both lung and liver does not affect long-term hepatic accumulation following pulmonary exposure, *PLoS One*, 2018, **13**, e0202477.

120 H. K. Sung, E. Jo, E. Kim, S. K. Yoo, J. W. Lee, P. J. Kim, Y. Kim and I. C. Eom, Analysis of gold and silver nanoparticles internalized by zebrafish (Danio rerio) using single particle-inductively coupled plasma-mass spectrometry, *Chemosphere*, 2018, **209**, 815–822.

121 M. V. Taboada-López, S. Iglesias-López, P. Herbello-Hermelo, P. Bermejo-Barrera and A. Moreda-Piñeiro, Ultrasound assisted enzymatic hydrolysis for isolating titanium dioxide nanoparticles from bivalve mollusk before sp-ICP-MS, *Anal. Chim. Acta*, 2018, **1018**, 16–25.

122 F. Abdolahpur Monikh, L. Chupani, E. Zuskova, R. Peters, M. Vancová, M. G. Vijver, P. Porcal and W. J. Peijnenburg, Method for extraction and quantification of metal-based nanoparticles in biological media: number-based biodistribution and bioconcentration, *Environ. Sci. Technol.*, 2019, **53**, 946–953.

123 S. Hu, R. Liu, S. Zhang, Z. Huang, Z. Xing and X. Zhang, A new strategy for highly sensitive immunoassay based on single-particle mode detection by inductively coupled plasma mass spectrometry, *J. Am. Soc. Mass Spectrom.*, 2009, **20**, 1096–1103.

124 S. Zhang, G. Han, Z. Xing, S. Zhang and X. Zhang, Multiplex DNA assay based on nanoparticle probes by single particle inductively coupled plasma mass spectrometry, *Anal. Chem.*, 2014, **86**, 3541–3547.

125 H. Klingberg, L. B. Oddershede, K. Loeschner, E. H. Larsen, S. Loft and P. Møller, Uptake of gold nanoparticles in primary human endothelial cells, *Toxicol. Res.*, 2015, **4**, 655–666.

126 I. L. Hsiao, F. S. Bierkandt, P. Reichardt, A. Luch, Y. J. Huang, N. Jakubowski, J. Tentschert and A. Haase, Quantification and visualization of cellular uptake of TiO_2 and Ag nanoparticles: comparison of different ICP-MS techniques, *J. Nanobiotechnol.*, 2016, **14**, 50.

127 A. Malysheva, N. Voelcker, P. E. Holm and E. Lombi, Unraveling the complex behavior of AgNPs driving NP-cell interactions and toxicity to algal cells, *Environ. Sci. Technol.*, 2016, **50**, 12455–12463.

128 B. Krause, T. Meyer, H. Sieg, C. Kästner, P. Reichardt, J. Tentschert, H. Jungnickel, I. Estrela-Lopis, A. Burel, S. Chevance, F. Gauffre, P. Jalili, J. Meijer, L. Böhmert, A. Braeuning, A. F. Thünemann, F. Emmerling, V. Fessard, P. Laux, A. Lampen and A. Luch, Characterization of aluminum, aluminum oxide and titanium dioxide nanomaterials using a combination of methods for particle surface and size analysis, *RSC Adv.*, 2018, **8**, 14377–14388.

129 I. Aharchaou, J. S. Py, S. Cambier, J. L. Loizeau, G. Cornelis, P. Rousselle, E. Battaglia and D. A. L. Vignati, Chromium hazard and risk assessment: New insights from a detailed speciation study in a standard test medium, *Environ. Toxicol. Chem.*, 2018, **37**, 983–992.

130 X. Xu, J. Chen, B. Li, L. Tang and J. Jiang, Single particle ICP-MS-based absolute and relative quantification of E. coli O157 16S rRNA using sandwich hybridization capture, *Analyst*, 2019, **144**, 1725–1730.

131 A. P. Walczak, R. Fokkink, R. Peters, P. Tromp, Z. E. Herrera Rivera, I. M. Rietjens, P. J. Hendriksen and H. Bouwmeester, Behaviour of silver nanoparticles and silver ions in an *in vitro* human gastrointestinal digestion model, *Nanotoxicology*, 2013, **7**, 1198–1210.

132 S. V. Jenkins, H. Qu, T. Mudalige, T. M. Ingle, R. Wang, F. Wang, P. C. Howard, J. Chen and Y. Zhang, Rapid determination of plasmonic nanoparticle agglomeration status in blood, *Biomaterials*, 2015, **51**, 226–237.

133 E. Leese, J. F. Staff, V. A. Carolan and J. Morton, Exhaled breath condensate: a novel matrix for biological monitoring to assess occupational exposure to respirable crystalline silica, *Ann. Work Exposures Health*, 2017, **61**, 902–906.

134 M. Witzler, F. Küllmer and K. Günther, Validating a single-particle ICP-MS method to measure nanoparticles in human whole blood for nanotoxicology, *Anal. Lett.*, 2017, **51**, 587–599.

135 J. Vidmar, T. Buerki-Thurnherr and K. Loeschner, Comparison of the suitability of alkaline or enzymatic sample pre-treatment for characterization of silver nanoparticles in human tissue by single particle ICP-MS, *J. Anal. At. Spectrom.*, 2018, **33**, 752–761.

136 J. Vidmar, K. Loeschner, M. Correia, E. H. Larsen, P. Manser, A. Wichser, K. Boodhia, Z. S. Al-Ahmady, J. Ruiz, D. Astruc and T. Buerki-Thurnherr, Translocation of silver nanoparticles in the ex vivo human placenta perfusion model characterized by single particle ICP-MS, *Nanoscale*, 2018, **10**, 11980–11991.

137 M. Logozzi, D. Mizzoni, B. Bocca, R. Di Raimo, F. Petrucci, S. Caimi, A. Alimonti, M. Falchi, F. Cappello, C. Campanella, C. C. Bavisotto, S. David, F. Bucchieri,

D. F. Angelini, L. Battistini and S. Fais, Human primary macrophages scavenge AuNPs and eliminate it through exosomes. A natural shuttling for nanomaterials, *Eur. J. Pharm. Biopharm.*, 2019, **137**, 23–36.

138 R. B. Reed, D. G. Goodwin, K. L. Marsh, S. S. Capracotta, C. P. Higgins, D. H. Fairbrother and J. F. Ranville, Detection of single walled carbon nanotubes by monitoring embedded metals, *Environ. Sci.: Processes Impacts*, 2013, **15**, 204–213.

139 J. J. Wang, R. S. Lankone, R. B. Reed, D. H. Fairbrother and J. F. Ranville, Analysis of single-walled carbon nanotubes using spICP-MS with microsecond dwell time, *NanoImpact*, 2016, **1**, 65–72.

140 R. S. Lankone, J. Wang, J. F. Ranville and D. H. Fairbrother, Photodegradation of polymer-CNT nanocomposites: effect of CNT loading and CNT release characteristics, *Environ. Sci.: Nano*, 2017, **4**, 967–982.

141 Y. Dan, H. Shi, C. Stephan and X. Liang, Rapid analysis of titanium dioxide nanoparticles in sunscreens using single particle inductively coupled plasma–mass spectrometry, *Microchem. J.*, 2015, **122**, 119–126.

142 I. de la Calle, M. Menta, M. Klein and F. Seby, Screening of TiO_2 and Au nanoparticles in cosmetics and determination of elemental impurities by multiple techniques (DLS, SP-ICP-MS, ICP-MS and ICP-OES), *Talanta*, 2017, **171**, 291–306.

143 B. Bocca, S. Caimi, O. Senofonte, A. Alimonti and F. Petrucci, ICP-MS based methods to characterize nanoparticles of TiO_2 and ZnO in sunscreens with focus on regulatory and safety issues, *Sci. Total Environ.*, 2018, **630**, 922–930.

144 I. de la Calle, M. Menta, M. Klein, B. Maxit and F. Séby, Towards routine analysis of TiO_2 (nano-)particle size in consumer products: Evaluation of potential techniques, *Spectrochim. Acta, Part B*, 2018, **147**, 28–42.

145 P. J. Lu, S. W. Fang, W. L. Cheng, S. C. Huang, M. C. Huang and H. F. Cheng, Characterization of titanium dioxide and zinc oxide nanoparticles in sunscreen powder by comparing different measurement methods, *J. Food Drug Anal.*, 2018, **26**, 1192–1200.

146 M. Correia, T. Uusimäki, A. Philippe and K. Loeschner, Challenges in determining the size distribution of nanoparticles in consumer products by asymmetric flow field-flow fractionation coupled to inductively coupled plasma-mass spectrometry: the example of Al_2O_3, TiO_2, and SiO_2 nanoparticles in toothpaste, *Separations*, 2018, **5**, 56.

147 Y. S. Zimmermann, A. Schaffer, P. F. Corvini and M. Lenz, Thin-film photovoltaic cells: long-term metal(loid) leaching at their end-of-life, *Environ. Sci. Technol.*, 2013, **47**, 13151–13159.

148 L. M. Furtado, M. E. Hoque, D. F. Mitrano, J. F. Ranville, B. Cheever, P. C. Frost, M. A. Xenopoulos, H. Hintelmann and C. D. Metcalfe, The persistence and transformation of silver nanoparticles in littoral lake mesocosms monitored using various analytical techniques, *Environ. Chem.*, 2014, **11**, 419–430.

149 D. M. Mitrano, J. F. Ranville, A. Bednar, K. Kazor, A. S. Hering and C. P. Higgins, Tracking dissolution of silver nanoparticles at environmentally relevant concentrations in laboratory, natural, and processed waters using single particle ICP-MS (spICP-MS), *Environ. Sci.: Nano*, 2014, **1**, 248–259.

150 A. R. Donovan, C. D. Adams, Y. Ma, C. Stephan, T. Eichholz and H. Shi, Detection of zinc oxide and cerium dioxide nanoparticles during drinking water treatment by rapid single particle ICP-MS methods, *Anal. Bioanal. Chem.*, 2016, **408**, 5137–5145.

151 A. R. Donovan, C. D. Adams, Y. Ma, C. Stephan, T. Eichholz and H. Shi, Single particle ICP-MS characterization of titanium dioxide, silver, and gold nanoparticles during drinking water treatment, *Chemosphere*, 2016, **144**, 148–153.

152 M. Azodi, Y. Sultan and S. Ghoshal, Dissolution behavior of silver nanoparticles and formation of secondary silver nanoparticles in municipal wastewater by single-particle ICP-MS, *Environ. Sci. Technol.*, 2016, **50**, 13318–13327.

153 J. Jiménez-Lamana and V. I. Slaveykova, Silver nanoparticle behaviour in lake water depends on their surface coating, *Sci. Total Environ.*, 2016, **573**, 946–953.

154 C.-l. Long, Z.-g. Yang, Y. Yang, H.-p. Li and Q. Wang, Determination of gold nanoparticles in natural water using single particle-ICP-MS, *J. Cent. South Univ.*, 2016, **23**, 1611–1617.

155 J. M. Pettibone and J. Liu, *In situ* methods for monitoring silver nanoparticle sulfidation in simulated waters, *Environ. Sci. Technol.*, 2016, **50**, 11145–11153.

156 L. Telgmann, M. T. Nguyen, L. Shen, V. Yargeau, H. Hintelmann and C. D. Metcalfe, Single particle ICP-MS as a tool for determining the stability of silver nanoparticles in aquatic matrixes under various environmental conditions, including treatment by ozonation, *Anal. Bioanal. Chem.*, 2016, **408**, 5169–5177.

157 A. Azimzada, N. Tufenkji and K. J. Wilkinson, Transformations of silver nanoparticles in wastewater effluents: links to Ag bioavailability, *Environ. Sci.: Nano*, 2017, **4**, 1339–1349.

158 R. Aznar, F. Barahona, O. Geiss, J. Ponti, T. Jose Luis and J. Barrero-Moreno, Quantification and size characterisation of silver nanoparticles in environmental aqueous samples and consumer products by single particle-ICPMS, *Talanta*, 2017, **175**, 200–208.

159 Y. J. Chang, Y. H. Shih, C. H. Su and H. C. Ho, Comparison of three analytical methods to measure the size of silver nanoparticles in real environmental water and wastewater samples, *J. Hazard. Mater.*, 2017, **322**, 95–104.

160 N. Londono, A. R. Donovan, H. Shi, M. Geisler and Y. Liang, Impact of TiO_2 and ZnO nanoparticles on an aquatic microbial community: effect at environmentally relevant concentrations, *Nanotoxicology*, 2017, **11**, 1140–1156.

161 J. D. Martin, L. Telgmann and C. D. Metcalfe, A method for preparing silver nanoparticle suspensions in bulk for ecotoxicity testing and ecological risk assessment, *Bull. Environ. Contam. Toxicol.*, 2017, **98**, 589–594.

162 R. C. Merrifield, C. Stephan and J. Lead, Determining the concentration dependent transformations of Ag nanoparticles in complex media: using SP-ICP-MS and Au@Ag core-shell nanoparticles as tracers, *Environ. Sci. Technol.*, 2017, **51**, 3206–3213.

163 T. Théoret and K. J. Wilkinson, Evaluation of enhanced darkfield microscopy and hyperspectral analysis to analyse the fate of silver nanoparticles in wastewaters, *Anal. Methods*, 2017, **9**, 3920–3928.

164 C. Toncelli, K. Mylona, I. Kalantzi, A. Tsiola, P. Pitta, M. Tsapakis and S. A. Pergantis, Silver nanoparticles in seawater: A dynamic mass balance at part per trillion silver concentrations, *Sci. Total Environ.*, 2017, **601–602**, 15–21.

165 L. Degenkolb, G. Metreveli, A. Philippe, A. Brandt, K. Leopold, L. Zehlike, H. J. Vogel, G. E. Schaumann, T. Baumann, M. Kaupenjohann, F. Lang, S. Kumahor and S. Klitzke, Retention and remobilization mechanisms of environmentally aged silver nanoparticles in an artificial riverbank filtration system, *Sci. Total Environ.*, 2018, **645**, 192–204.

166 A. R. Donovan, C. D. Adams, Y. Ma, C. Stephan, T. Eichholz and H. Shi, Fate of nanoparticles during alum and ferric coagulation monitored using single particle ICP-MS, *Chemosphere*, 2018, **195**, 531–541.

167 A. Georgantzopoulou, P. Almeida Carvalho, C. Vogelsang, M. Tilahun, K. Ndungu, A. M. Booth, K. V. Thomas and A. Macken, Ecotoxicological effects of transformed silver and titanium dioxide nanoparticles in the effluent from a lab-scale wastewater treatment system, *Environ. Sci. Technol.*, 2018, **52**, 9431–9441.

168 L. Luo, Y. Yang, H. Li, R. Ding, Q. Wang and Z. Yang, Size characterization of silver nanoparticles after separation from silver ions in environmental water using magnetic reduced graphene oxide, *Sci. Total Environ.*, 2018, **612**, 1215–1222.

169 J. D. Martin, P. C. Frost, H. Hintelmann, K. Newman, M. J. Paterson, L. Hayhurst, M. D. Rennie, M. A. Xenopoulos, V. Yargeau and C. D. Metcalfe, Accumulation of silver in yellow perch (Perca flavescens) and northern pike (Esox lucius) From a lake dosed with nanosilver, *Environ. Sci. Technol.*, 2018, **52**, 11114–11122.

170 D. C. Rearick, L. Telgmann, H. Hintelmann, P. C. Frost and M. A. Xenopoulos, Spatial and temporal trends in the fate of silver nanoparticles in a whole-lake addition study, *PLoS One*, 2018, **13**, e0201412.

171 J. Vidmar, P. Oprčkal, R. Milačič, A. Mladenovič and J. Ščančar, Investigation of the behaviour of zero-valent iron nanoparticles and their interactions with Cd(2+) in wastewater by single particle ICP-MS, *Sci. Total Environ.*, 2018, **634**, 1259–1268.

172 J. J. López-Mayán, B. Cerneira-Temperán, E. Peña-Vázquez, M. C. Barciela-Alonso, M. R. Domínguez-González and P. Bermejo-Barrera, Evaluation of a cloud point extraction method for the preconcentration and quantification of silver nanoparticles in water samples by ETAAS, *Int. J. Environ. Anal. Chem.*, 2019, **98**, 1434–1447.

173 A. P. Gondikas, F. von der Kammer, R. B. Reed, S. Wagner, J. F. Ranville and T. Hofmann, Release of TiO_2 nanoparticles from sunscreens into surface waters: a one-year survey at the old Danube recreational Lake, *Environ. Sci. Technol.*, 2014, **48**, 5415–5422.

174 M. Hadioui, V. Merdzan and K. J. Wilkinson, Detection and characterization of ZnO nanoparticles in surface and waste waters using single particle ICPMS, *Environ. Sci. Technol.*, 2015, **49**, 6141–6148.

175 L. Li, M. Stoiber, A. Wimmer, Z. Xu, C. Lindenblatt, B. Helmreich and M. Schuster, To what extent can full-scale wastewater treatment plant effluent influence the occurrence of silver-based nanoparticles in surface waters?, *Environ. Sci. Technol.*, 2016, **50**, 6327–6333.

176 S. P. Bitragunta, S. G. Palani, A. Gopala, S. K. Sarkar and V. R. Kandukuri, Detection of TiO_2 nanoparticles in municipal sewage treatment plant and their characterization using single particle ICP-MS, *Bull. Environ. Contam. Toxicol.*, 2017, **98**, 595–600.

177 R. B. Reed, D. P. Martin, A. J. Bednar, M. D. Montaño, P. Westerhoff and J. F. Ranville, Multi-day diurnal measurements of Ti-containing nanoparticle and organic sunscreen chemical release during recreational use of a natural surface water, *Environ. Sci.: Nano*, 2017, **4**, 69–77.

178 M. Loula, A. Kaňa, R. Koplík, J. Hanuš, M. Vosmanská and O. Mestek, Analysis of silver nanoparticles using single-particle inductively coupled plasma – mass spectrometry (ICP-MS): parameters affecting the quality of results, *Anal. Lett.*, 2018, **52**, 288–307.

179 C. D. Metcalfe, T. Sultana, J. Martin, K. Newman, P. Helm, S. Kleywegt, L. Shen and V. Yargeau, Silver near municipal wastewater discharges into western Lake Ontario, Canada, *Environ. Monit. Assess.*, 2018, **190**, 555.

180 R. J. B. Peters, G. van Bemmel, N. B. L. Milani, G. C. T. den Hertog, A. K. Undas, M. van der Lee and H. Bouwmeester, Detection of nanoparticles in Dutch surface waters, *Sci. Total Environ.*, 2018, **621**, 210–218.

181 A. K. Venkatesan, R. B. Reed, S. Lee, X. Bi, D. Hanigan, Y. Yang, J. F. Ranville, P. Herckes and P. Westerhoff, Detection and sizing of Ti-containing particles in recreational waters using single particle ICP-MS, *Bull. Environ. Contam. Toxicol.*, 2018, **100**, 120–126.

182 A. Wimmer, A. Kalinnik and M. Schuster, New insights into the formation of silver-based nanoparticles under natural and semi-natural conditions, *Water Res.*, 2018, **141**, 227–234.

183 A. K. Venkatesan, B. T. Rodríguez, A. R. Marcotte, X. Bi, J. Schoepf, J. F. Ranville, P. Herckes and P. Westerhoff, Using single-particle ICP-MS for monitoring metal-containing particles in tap water, *Environ. Sci.: Water Res. Technol.*, 2018, **4**, 1923–1932.

184 F. Loosli, J. Wang, S. Rothenberg, M. Bizimis, C. Winkler, O. Borovinskaya, L. Flamigni and M. Baalousha, Sewage spills are a major source of titanium dioxide engineered (nano)-particle release into the environment, *Environ. Sci.: Nano*, 2019, **6**, 763–777.

185 R. J. B. Peters, Z. H. Rivera, H. Bouwmeester, S. Weigel and H. J. P. Marvin, Advanced analytical techniques for the measurement of nanomaterials in complex samples: a comparison, *Qual. Assur. Saf. Crops*, 2014, **6**, 281–290.

186 S. Addo Ntim, T. A. Thomas and G. O. Noonan, Influence of aqueous food simulants on potential nanoparticle detection in migration studies involving nanoenabled food-contact substances, *Food Addit. Contam., Part A*, 2016, **33**, 905–912.

187 M. Witzler, F. Kullmer, A. Hirtz and K. Günther, Validation of gold and silver nanoparticle analysis in fruit juices by single-particle ICP-MS without sample pretreatment, *J. Agric. Food Chem.*, 2016, **64**, 4165–4170.

188 M. Jokar, M. Correia and K. Loeschner, Behavior of silver nanoparticles and ions in food simulants and low fat cow milk under migration conditions, *Food Control*, 2018, **89**, 77–85.

189 R. J. Peters, G. van Bemmel, Z. Herrera-Rivera, H. P. Helsper, H. J. Marvin, S. Weigel, P. C. Tromp, A. G. Oomen, A. G. Rietveld and H. Bouwmeester, Characterization of titanium dioxide nanoparticles in food products: analytical methods to define nanoparticles, *J. Agric. Food Chem.*, 2014, **62**, 6285–6293.

190 E. Verleysen, E. Van Doren, N. Waegeneers, P. J. De Temmerman, M. Abi Daoud Francisco and J. Mast, TEM and SP-ICP-MS analysis of the release of silver nanoparticles from decoration of pastry, *J. Agric. Food Chem.*, 2015, **63**, 3570–3578.

191 I. de la Calle, M. Menta, M. Klein and F. Seby, Study of the presence of micro- and nanoparticles in drinks and foods by multiple analytical techniques, *Food Chem.*, 2018, **266**, 133–145.

192 K. Loeschner, M. Correia, C. Lopez Chaves, I. Rokkjaer and J. J. Sloth, Detection and characterisation of aluminium-containing nanoparticles in Chinese noodles by single particle ICP-MS, *Food Addit. Contam., Part A*, 2018, **35**, 86–93.

193 M. V. Taboada-López, P. Herbello-Hermelo, R. Domínguez-González, P. Bermejo-Barrera and A. Moreda-Piñeiro, Enzymatic hydrolysis as a sample pre-treatment for titanium dioxide nanoparticles assessment in surimi (crab sticks) by single particle ICP-MS, *Talanta*, 2019, **195**, 23–32.

194 Y. Dan, W. Zhang, R. Xue, X. Ma, C. Stephan and H. Shi, Characterization of gold nanoparticle uptake by tomato plants using enzymatic extraction followed by single-particle inductively coupled plasma-mass spectrometry analysis, *Environ. Sci. Technol.*, 2015, **49**, 3007–3014.

195 D. Bao, Z. G. Oh and Z. Chen, Characterization of silver nanoparticles internalized by arabidopsis plants using single particle ICP-MS analysis, *Front. Plant Sci.*, 2016, **7**, 32.

196 Y. Dan, X. Ma, W. Zhang, K. Liu, C. Stephan and H. Shi, Single particle ICP-MS method development for the determination of plant uptake and accumulation of CeO_2 nanoparticles, *Anal. Bioanal. Chem.*, 2016, **408**, 5157–5167.

197 J. Jiménez-Lamana, J. Wojcieszek, M. Jakubiak, M. Asztemborska and J. Szpunar, Single particle ICP-MS characterization of platinum nanoparticles uptake and bioaccumulation by *Lepidium sativum* and *Sinapis alba* plants, *J. Anal. At. Spectrom.*, 2016, **31**, 2321–2329.

198 I. D. la Calle, P. Pérez-Rodríguez, D. Soto-Gómez and J. E. López-Periago, Detection and characterization of Cu-bearing particles in throughfall samples from vine leaves by DLS, AF4-MALLS (-ICP-MS) and SP-ICP-MS, *Microchem. J.*, 2017, **133**, 293–301.

199 C. C. Li, F. Dang, M. Li, M. Zhu, H. Zhong, H. Hintelmann and D. M. Zhou, Effects of exposure pathways on the accumulation and phytotoxicity of silver nanoparticles in soybean and rice, *Nanotoxicology*, 2017, **11**, 699–709.

200 P. Wang, E. Lombi, S. Sun, K. G. Scheckel, A. Malysheva, B. A. McKenna, N. W. Menzies, F.-J. Zhao and P. M. Kopittke, Characterizing the uptake, accumulation and toxicity of silver sulfide nanoparticles in plants, *Environ. Sci.: Nano*, 2017, **4**, 448–460.

201 A. A. Keller, Y. Huang and J. Nelson, Detection of nanoparticles in edible plant tissues exposed to nano-copper using single-particle ICP-MS, *J. Nanoparticle Res.*, 2018, **20**.

202 K. Kinska, J. Jiménez-Lamana, J. Kowalska, B. Krasnodebska-Ostrega and J. Szpunar, Study of the uptake and bioaccumulation of palladium nanoparticles by Sinapis alba using single particle ICP-MS, *Sci. Total Environ.*, 2018, **615**, 1078–1085.

203 S. S. D. Kumar, N. N. Houreld, E. M. Kroukamp and H. Abrahamse, Cellular imaging and bactericidal mechanism of green-synthesized silver nanoparticles against human pathogenic bacteria, *J. Photochem. Photobiol. B*, 2018, **178**, 259–269.

204 J. Nath, I. Dror, P. Landa, T. Vanek, I. Kaplan-Ashiri and B. Berkowitz, Synthesis and characterization of isotopically-labeled silver, copper and zinc oxide nanoparticles for tracing studies in plants, *Environ. Pollut.*, 2018, **242**, 1827–1837.

205 H. Zhang, Y. Huang, J. Gu, A. Keller, Y. Qin, Y. Bian, K. Tang, X. Qu, R. Ji and L. Zhao, Single particle ICP-MS and GC-MS provide a new insight into the formation mechanisms during the green synthesis of AgNPs, *New J. Chem.*, 2019, **43**, 3946–3955.

206 J. Wojcieszek, J. Jiménez-Lamana, K. Bierla, M. Asztemborska, L. Ruzik, M. Jarosz and J. Szpunar, Elucidation of the fate of zinc in model plants using single particle ICP-MS and ESI tandem MS, *J. Anal. At. Spectrom.*, 2019, **34**, 683–693.

207 Y. Yang, X. Bi, P. Westerhoff, K. Hristovski and J. E. McLain, Engineered nanomaterials impact biological carbon conversion in soils, *Environ. Eng. Sci.*, 2014, **31**, 381–392.

208 J. Navratilova, A. Praetorius, A. Gondikas, W. Fabienke, F. von der Kammer and T. Hofmann, Detection of engineered copper nanoparticles in soil using single particle ICP-MS, *Int. J. Environ. Res. Public Health*, 2015, **12**, 15756–15768.

209 H. E. Hadri and V. A. Hackley, Investigation of cloud point extraction for the analysis of metallic nanoparticles in a soil matrix, *Environ. Sci.: Nano*, 2017, **4**, 105–116.

210 A. H. Jesmer, J. R. Velicogna, D. M. Schwertfeger, R. P. Scroggins and J. I. Princz, The toxicity of silver to soil organisms exposed to silver nanoparticles and silver nitrate in biosolids-amended field soil, *Environ. Toxicol. Chem.*, 2017, **36**, 2756–2765.

211 D. Schwertfeger, J. Velicogna, A. Jesmer, H. McShane, R. Scroggins and J. Princz, Ion exchange technique (IET) to characterise Ag^+ exposure in soil extracts contaminated with engineered silver nanoparticles, *Environ. Chem.*, 2017, **14**, 123–133.

212 D. M. Schwertfeger, J. R. Velicogna, A. H. Jesmer, S. Saatcioglu, H. McShane, R. P. Scroggins and J. I. Princz, Extracting metallic nanoparticles from soils for quantitative analysis: method development using engineered silver nanoparticles and SP-ICP-MS, *Anal. Chem.*, 2017, **89**, 2505–2513.

213 H. El Hadri, S. M. Louie and V. A. Hackley, Assessing the interactions of metal nanoparticles in soil and sediment matrices – a quantitative analytical multi-technique approach, *Environ. Sci.: Nano*, 2018, **5**, 203–214.

214 L. Torrent, M. Iglesias, M. Hidalgo and E. Marguí, Determination of silver nanoparticles in complex aqueous matrices by total reflection X-ray fluorescence spectrometry combined with cloud point extraction, *J. Anal. At. Spectrom.*, 2018, **33**, 383–394.

215 M. A. Gomez-Gonzalez, E. Bolea, P. A. O'Day, J. Garcia-Guinea, F. Garrido and F. Laborda, Combining single-particle inductively coupled plasma mass spectrometry and X-ray absorption spectroscopy to evaluate the release of colloidal arsenic from environmental samples, *Anal. Bioanal. Chem.*, 2016, **408**, 5125–5135.

216 F. Tou, Y. Yang, J. Feng, Z. Niu, H. Pan, Y. Qin, X. Guo, X. Meng, M. Liu and M. F. Hochella, Environmental risk implications of metals in sludges from waste water treatment plants: the discovery of vast stores of metal-containing nanoparticles, *Environ. Sci. Technol.*, 2017, **51**, 4831–4840.

217 K. Folens, T. Van Acker, E. Bolea-Fernandez, G. Cornelis, F. Vanhaecke, G. Du Laing and S. Rauch, Identification of platinum nanoparticles in road dust leachate by single particle inductively coupled plasma-mass spectrometry, *Sci. Total Environ.*, 2018, **615**, 849–856.

218 Z. Li, M. Hadioui and K. J. Wilkinson, Conditions affecting the release of thorium and uranium from the tailings of a niobium mine, *Environ. Pollut.*, 2019, **247**, 206–215.

219 M. Hadioui, S. Leclerc and K. J. Wilkinson, Multimethod quantification of Ag^+ release from nanosilver, *Talanta*, 2013, **105**, 15–19.

220 D. M. Mitrano, Y. Arroyo Rojas Dasilva and B. Nowack, Effect of variations of washing solution chemistry on nanomaterial physicochemical changes in the laundry cycle, *Environ. Sci. Technol.*, 2015, **49**, 9665–9673.

221 D. Paunescu, C. A. Mora, L. Querci, R. Heckel, M. Puddu, B. Hattendorf, D. Günther and R. N. Grass, Detecting and number counting of single engineered nanoparticles by digital particle polymerase chain reaction, *ACS Nano*, 2015, **9**, 9564–9572.

222 H. A. Kim, B. T. Lee, S. Y. Na, K. W. Kim, J. F. Ranville, S. O. Kim, E. Jo and I. C. Eom, Characterization of silver nanoparticle aggregates using single particle-inductively coupled plasma-mass spectrometry (spICP-MS), *Chemosphere*, 2017, **171**, 468–475.

223 A. S. Adeleye, E. A. Oranu, M. Tao and A. A. Keller, Release and detection of nanosized copper from a commercial antifouling paint, *Water Res.*, 2016, **102**, 374–382.

224 A. Mackevica, M. E. Olsson and S. F. Hansen, Silver nanoparticle release from commercially available plastic food containers into food simulants, *J. Nanoparticle Res.*, 2016, **18**, 5.

225 K. Ramos, M. M. Gómez-Gómez, C. Cámara and L. Ramos, Silver speciation and characterization of nanoparticles released from plastic food containers by single particle ICPMS, *Talanta*, 2016, **151**, 83–90.

226 D. P. Martin, N. L. Melby, S. M. Jordan, A. J. Bednar, A. J. Kennedy, M. E. Negrete, M. A. Chappell and A. R. Poda, Nanosilver conductive ink: A case study for evaluating the potential risk of nanotechnology under hypothetical use scenarios, *Chemosphere*, 2016, **162**, 222–227.

227 I. Abad-Alvaro, E. Bolea, F. Laborda and J. R. Castillo, An ICP-MS-based platform for release studies on silver-based nanomaterials, *J. Anal. At. Spectrom.*, 2017, **32**, 1101–1108.

228 A. Mackevica, M. E. Olsson and S. F. Hansen, The release of silver nanoparticles from commercial toothbrushes, *J. Hazard. Mater.*, 2017, **322**, 270–275.

229 A. Mackevica, M. E. Olsson and S. F. Hansen, Quantitative characterization of TiO_2 nanoparticle release from textiles by conventional and single particle ICP-MS, *J. Nanoparticle Res.*, 2017, **20**.

230 N. Neubauer, L. Scifo, J. Navratilova, A. Gondikas, A. Mackevica, D. Borschneck, P. Chaurand, V. Vidal, J. Rose, F. von der Kammer and W. Wohlleben, Nanoscale coloristic pigments: upper limits on releases from pigmented plastic during environmental aging, in food contact, and by leaching, *Environ. Sci. Technol.*, 2017, **51**, 11669–11680.

231 M. C. Sportelli, R. A. Picca, F. Paladini, A. Mangone, L. C. Giannossa, C. D. Franco, A. L. Gallo, A. Valentini, A. Sannino, M. Pollini and N. Cioffi, Spectroscopic characterization and nanosafety of Ag-modified antibacterial leather and leatherette, *Nanomaterials*, 2017, **7**, E203.

232 B. Bocca, E. Sabbioni, I. Mičetić, A. Alimonti and F. Petrucci, Size and metal composition characterization of nano- and microparticles in tattoo inks by a combination of analytical techniques, *J. Anal. At. Spectrom.*, 2017, **32**, 616–628.

233 J. Nelson, M. Yamanaka, F. Lopez-Linares, L. Poirier and E. Rogel, Characterization of dissolved metals and metallic nanoparticles in asphaltene solutions by single-particle inductively coupled plasma mass spectrometry, *Energy Fuels*, 2017, **31**, 11971–11976.

234 A. Sápi, A. Kéri, I. Kálomista, D. G. Dobó, Á. S. Ákos Szamosvölgyi, K. L. Juhász, Á. K. Ákos Kukovecz, Z. Kónya

and G. Galbács, Determination of the platinum concentration of a Pt/silica nanocomposite decorated with ultra small Pt nanoparticles using single particle inductively coupled plasma mass spectrometry, *J. Anal. At. Spectrom.*, 2017, **32**, 996–1003.

235 S. Addo Ntim, S. Norris, K. Scott, T. A. Thomas and G. O. Noonan, Consumer use effects on nanoparticle release from commercially available ceramic cookware, *Food Control*, 2018, **87**, 31–39.

236 J. Therkorn, L. Calderon, B. Cartledge, N. Thomas, B. Majestic and G. Mainelis, Inactivation of pure bacterial biofilms by impaction of aerosolized consumer products containing nanoparticulate metals, *Environ. Sci.: Nano*, 2018, **5**, 544–555.

237 R. D. Heringer and J. F. Ranville, Gunshot residue (GSR) analysis by single particle inductively coupled plasma mass spectrometry (spICP-MS), *Forensic Sci. Int.*, 2018, **288**, e20–e25.

238 J.-R. Huang, P. Li, J.-H. Wen, X. Hu, Y.-J. Chen, D.-H. Yin and H.-Z. Lian, Determination of arsenic species in mainstream cigarette smoke based on inductively coupled plasma mass spectrometry, *Spectrosc. Lett.*, 2018, **51**, 252–256.

239 J. Jiménez-Lamana, I. Abad-Álvaro, K. Bierla, F. Laborda, J. Szpunar and R. Lobinski, Detection and characterization of biogenic selenium nanoparticles in selenium-rich yeast by single particle ICPMS, *J. Anal. At. Spectrom.*, 2018, **33**, 452–460.

240 M. Van Wassenhoven, M. Goyens, E. Capieaux, P. Devos and P. Dorfman, Nanoparticle characterisation of traditional homeopathically manufactured Cuprum metallicum and Gelsemium sempervirens medicines and controls, *Homeopathy*, 2018, **107**, 244–263.

241 A. Hegetschweiler, O. Borovinskaya, T. Staudt and T. Kraus, Single particle mass spectrometry of titanium and niobium carbonitride precipitates in steels, *Anal. Chem.*, 2018, **91**, 943–950.